Smartphone-based 3D Scanning and Image Processing for Ostomy Wafer Customization

Francisco Luquin Monroy

A thesis

submitted in partial fulfillment of the

requirements for the degree of

Master of Science in Electrical Engineering

University of Washington

2023

Committee:

Rania Hussein

Alexander Mamishev

Program Authorized to Offer Degree:

Electrical and Computer Engineering

University of Washington

Abstract

Smartphone-based 3D Scanning and Image Processing for Ostomy Wafer Customization

Francisco Luquin Monroy

Chair of the Supervisory Committee:

Rania Hussein

Department of Electrical and Computer Engineering

Millions of ostomy patients rely on outdated tools to adjust their wafers, which must fit around their stoma. The stoma can be described as a surgically created hole in a patient's abdomen, from which the patient's intestinal or urinary tract will divert bodily waste. One of the purposes of ostomy wafers is to protect the surrounding skin from bodily waste, and incorrectly fitting the wafers can lead to many complications. For example, a tightly fitting wafer can cut into the nerveless intestine, leading to unnoticed excessive bleeding. Conversely, a loosely fitting wafer exposes skin to bodily waste, which can result in skin erosion and infection. Recognizing the need for better tools for ostomy patients, we are developing Osto-Mate, a system utilizing smartphones with depth-sensing capabilities, to provide ostomy patients with customized wafers. This thesis explores the characterization of the iPhone's TrueDepth sensor to confirm its suitability as a 3D scanning device for the system and introduces a method for extracting stoma model contours from 2.5D images. It further discusses the design and functionality of the application, illustrating its

potential to improve the process of ostomy wafer fitting. Preliminary tests show promising results for enhancing the accuracy of wafer adjustment, paving the way for improved patient safety and convenience.

ACKNOWLEDGEMENTS

Firstly, I would like to express my deepest gratitude to my advisor Prof. Rania Hussein. From the early days of my sophomore year, her belief in my potential and encouragement to pursue graduate school has significantly shaped my path in life. She has given me the opportunity to join her Remote Hub Lab to undertake research on a real-world project, lead a team of student researchers, and learn about the process of commercialization, all while fostering a culture of rigorous research. The countless hours spent side by side, refining manuscripts and refining research directions has not only enriched my professional growth but has also allowed me to witness firsthand the dedication required to drive research from inception to publication. Her mentorship has been a cornerstone of my journey, instilling in me the values of persistence, intellectual curiosity, and collaborative spirit. This has provided me with an invaluable education in all the aspects I could have hoped for.

I am deeply appreciative of the mentorship Dr. Alexander Mamishev has provided me, particularly during my initial year. The experience of conducting research in his lab has helped me develop the skills to methodically break down complex projects into simple and straightforward tasks—although not easy, as nothing can change that. A significant portion of my research, writing, and commercialization knowledge was developed under his guidance.

As the project aims to transcend the bounds of the Remote Hub lab, the valuable expertise contributed by numerous individuals deserves acknowledgment. I want to extend my thanks to Nurse Practitioner Quyen Stevenson, whose rich experience in the medical field has been instrumental in guiding and refining this project. Thanks are due to Dr. Forest Bohrer, who assisted us in navigating the complexities of intellectual property and commercialization. I am indebted to Dr. Terri Butler, who has generously provided her expertise in life sciences and commercialization and committed her time and effort to mentor us during the NSF I-Corps program. I would also like to express my appreciation to the ostomy patients, WOC nurses, doctors, and industry professionals who graciously gave us their time for interviews, enabling us to refine the project further.

A project of this magnitude is not an endeavor one can undertake alone. I am grateful to the dedicated student team who propelled this project to its current stage: Stefhany Alves Ferreira, Sean Lim, Sai Jayanth Kalisi, Kashish Aggarwal, Masaya Takasaki, Nuha Qadir, Graciela Bracamontes Olivares, Thompson Ngo, and Kriti Bhardwaj. I am also grateful to all my fellow researchers at the Remote Hub Lab, whose collaborative spirit and shared passion for pushing boundaries have made my research endeavors truly enriching.

This material is based upon work supported by the National Science Foundation under Grant No. 2229218. Many thanks to the University of Washington's Royalty Research Fund, whose grant was crucial in developing this project. Additionally, I extend my appreciation to the faculty and staff of the ECE department for their support during my academic journey.

Finally, I would not have made it this far without the love and support of my family and friends. Special thanks to my wife, mom, and sister, whose endless encouragement and comforting words have helped me keep my sanity. Your support has made all the difference.

TABLE OF CONTENTS

Chapter 1. INTRODUCTION

This research was initiated by the perceived need to assist elderly ostomy patients facing potential difficulties with visual acuity and dexterity in adjusting their medical appliances. Our initial proposition was to develop a smartphone-based system aimed at helping these patients customize their wafers more easily.

As development proceeded, we concurrently conducted interviews, revealing that the issue may not be as widespread as initially assumed. However, we still see value in exploring and developing this technology, as it can serve as a supplementary tool for those who might benefit from it and as a step forward in digital health solutions for ostomy care.

This thesis delves into the development of the proposed application, with a strong focus on user-centric design and implementing the iPhone's TrueDepth sensors for scanning purposes. It also delves into a rules-based algorithm for extracting contours from 2.5D images, offering a novel method to capture and represent the detailed structure of stomas.

This research, encapsulated in the thesis, builds upon and expands the work previously published by the author in [1] and [2]. While it may serve a smaller audience than initially anticipated, it nonetheless establishes a foundation for future research and innovation in digital health solutions for ostomy care.

1.1 Introduction to Ostomy Wafer Fitting

Approximately 1 million individuals in the United States live with an ostomy [3, 4], with an additional 100,000 surgeries performed each year [3]. An ostomy is a surgically created opening in the intestinal or urinary tract to divert feces or urine from the body, typically necessitated by conditions such as injury or cancer [4, 5]. Given the necessity for fecal or urine expulsion through the ostomy, patients must regularly maintain their ostomy site, which can remain in place anywhere from a few months to permanently, depending on the nature of the underlying condition. Proper stoma care is crucial for an ostomate's overall well-being and health-related quality of life (HRQoL) [6-9]. Consequences of suboptimal stoma management include skin irritation, leakage from the ostomy bag, restricted mobility, pain, and social difficulties [10-13]. The ostomy surgery process is illustrated in Figure 1.1.

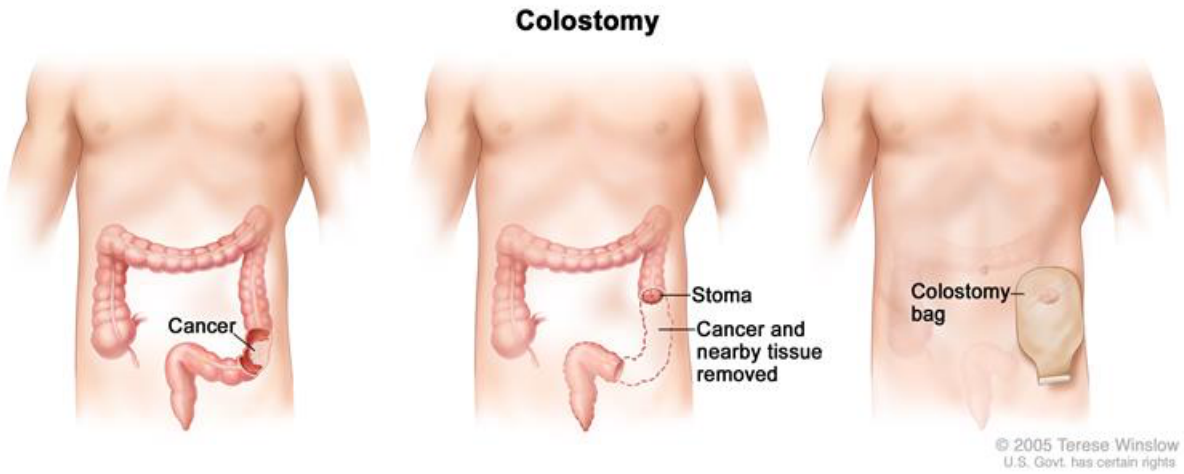

Figure 1.1: Sequential illustration of colon cancer diagnosis, colostomy procedure, and colostomy bag placement [14].

The maintenance process involves crucial steps, generally agreed upon within the ostomate community:

1) Assemble all necessary equipment: adhesive remover, ostomy wafer, ostomy pouch, ostomy belt, eakin seal, ostomy paste, face clothes, towels, and soap.
2) Remove the pouching system using adhesive remove pads. Use a removal wipe to remove the excess paste or seal on the skin around the stoma.
3) Wash the skin around the stoma using warm water and mild soap. Ensure all adhesive is washed off the skin. Rinse and dry skin well.
4) Cut the wafer according to the shape of the stoma. The wafer should be cut large enough to ensure that the wafer edges do not touch the stoma.
5) Apply a light dusting of ostomy powder to any reddened skin. Seal the powder with a barrier wipe. Allow the barrier wipe time to air dry (~ 2 seconds).
6) Mold an eakin seal snugly around the stoma.
7) Remove the plastic backing on the wafer.
8) Remove the tape border edge on the wafer and apply it around the stoma, ensuring there are no wrinkles.,
9) Attach the pouch and make sure the pouch is securely fastened.
10) Place your hand over the pouching system to help connect the paste, eakin seal, and pouching system securely on the skin for a couple of minutes.
11) Attach the ostomy belt.

These steps were obtained from an image posted within an online community of ostomates on Facebook. The post is no longer retrievable, but the steps are confirmed with interviews conducted with numerous ostomates and are corroborated by official sources such as [15].

An integral part of ostomy management is applying an ostomy wafer. This adhesive silicon “sheet” accommodates the stoma and protects the surrounding skin, also known as the peristomal skin, from feces or urine. The ostomy wafer also serves as a platform to attach the ostomy bag. The wafer, typically worn at all times, must be replaced every two to seven days. The preparation

and positioning of the wafer pose particular challenges during the first two months post-surgery. This period is marked by significant changes in the healing ostomy site and a steep learning curve for patients. Typically, patients are still determining the products and processes that best suit their needs during this time.

Initially, our research was predicated on the hypothesis that the traditional method of customizing ostomy wafers, which involves using a paper template with circles of varying diameters (Figure 1.2), leads to significant difficulties for many patients. We posited that this method is time-consuming, and its potential inaccuracies could contribute to many stoma/peristomal complications that ostomates experience. Since stomas are rarely perfectly circular, inaccuracies in the wafer contour are likely. A large contour could expose peristomal skin to feces, leading to skin erosion, infections, or leakage. In contrast, wafers with a tightly fitting contour might inflect trauma and potentially cause bleeding and stoma suffocation. Consequently, we anticipated that a system facilitating precise wafer customization could significantly enhance ostomates' HRQoL. The critical aspect of this system is the accurate extraction of the stoma's contour.

Given the progress in imaging technology, we believe innovative tools can be designed to support ostomates adjusting to their post-surgery life. However, imaging technologies have been mainly applied to wound diagnosis and assessment, often utilizing 2D imaging methods. This approach presents a challenge as stomas are inherently three-dimensional, making it difficult to capture information accurately. Furthermore, 2D imaging is prone to errors and distortions arising from factors such as lighting, capture angle, and body curvature [16, 17]. To accurately capture the stoma's contour, images must be taken perpendicularly to the abdomen while mitigating factors affecting image quality, such as body creases or nearby hernias, common issues among ostomates [18].

The demands of 2D imaging pose significant challenges to potential users, raising concerns about its feasibility for individuals who need formal training. Therefore, there is a need for more reliable and user-friendly technology that allows for convenient at-home care without compromising on quality. Such a solution could have far-reaching impacts, extending to similar domains in healthcare and telehealth, like dermatology and burn management.

In addition to aiding patients in wafer customization, our interviews with ostomates have identified a significant gap in education and communication between patients and healthcare providers. Mobile technology could assist with wafer customization and management, education, and mental health support.

Figure 1.2: Individual with an ostomy evaluating stoma diameter using a reference circle guide

1.2 Existing Ostomy Wafer Fitting Process and Tools

Ostomy care has seen a range of stoma appliance products, each aimed at tackling specific issues patients face with their stoma management; however, they have yet to address the particular issue our research seeks to resolve effectively. Ostomy patients are tasked with customizing their ostomy wafers to accommodate their unique stoma shapes, which can vary greatly. The process typically involves determining the diameter of the stoma using a paper guide with circles of varying diameters and tracing this circle onto the ostomy wafer. However, this manual method can lead to the errors we discussed earlier.

An alternative is moldable wafers, which have a moldable center that can be rolled back to fit against the stoma. Although moldable wafers eliminate the need for customization, they are more expensive, can have a shorter lifespan, and leave behind adhesive residue that can be difficult and time-consuming to remove [19, 20]. Given their higher price and varying lifespan, these wafers are often reserved as a backup option for emergencies or travel [20].

Several alternatives, such as waste diversion devices [21] or waste blockers [21, 22], have been proposed to give users more control. However, these are either still in trial stages or have yet to gain widespread acceptance. Colostomy patients have the option of irrigation, which allows control over waste release timing, eliminating the need for a bag [3]. However, this method is limited to colostomy patients, who only make up a percentage of all ostomy patients, and not all are comfortable with this practice.

Through our interviews with over 150 patients and experts, we discovered that many who struggled with complications associated with ill-fitting wafers had devised a workaround. These patients cut the wafer larger than the stoma and use an eakin ring to fill the gap. This method

prevents the wafer from cutting into the intestine while safeguarding the skin from direct exposure to waste. Interestingly, many patients still encountered leakage regardless of how carefully they cut the wafer. Leakage occurs when waste enters the stoma-wafer gap and dissolves the wafer adhesive. However, using eakin rings resolved the issue.

This revelation provided valuable insight that enriched our understanding of the practical solutions patients employ in their ostomy care routines. While our project focused on improving wafer customization, these findings underscore the importance of understanding real-world practices and concerns within the ostomy patient community.

1.3 Review of 3D Reconstruction for Ostomy

Past research has delved into analyzing and measuring wounds using 2D imagery [23, 24] and 3D models constructed via structured light [25], stereophotogrammetry [26-28], 3D laser scanners [29-32], and other imaging methodologies [33-35]. For stoma imaging, the accuracy requirements are high due to the necessity for optimal cutting distances of 3.175 mm to 6.35 mm, depending on the stoma type. Thus, an error tolerance of around 2 mm is an appropriate goal prior to any clinical trials.

A 3D-based methodology is compelling because of its superior accuracy and robustness in representing objects with complex geometries. 2D imaging may not capture the stoma accurately as factors like lighting, angle of capture, and the stoma's complexity could influence the contour extracted. 3D reconstruction circumvents these issues, allowing for capturing the stoma in comprehensive detail without depending on exact positioning, lighting conditions, or requiring extensive user training.

However, scanning technology is typically costly, difficult to use, and generally lacks accessibility. Some modern smartphones have recently been developed with depth sensors, allowing for a comprehensive ostomy management system.

Within ostomy care, several studies have explored using various 3D scanners to assist ostomy patients in differing manners. For example, [30] examines the usage of Intel RealSense D415 and D435 camera systems for imaging stomas. In this research, the authors scanned three objects similar to a stoma of differing diameters (3, 6, and 9 cm) using the RealSense systems and a Picza 3D scanner. The Picza 3D scanner is used as a reference scanner because it has an accuracy of 0.1 mm. The models were positioned on a platform and scanned from various angles. A reference object on the platform is used to merge the scans. The findings suggest that 80% of points on the reconstructed models are within 3 mm from the ground truth. However, the study acknowledges the impracticality of the setup, and the models must be generated with guidance. Moreover, the error margin is too large for our project and could lead to stoma damage.

Research such as [36] characterizes eight scanning devices, including affordable options such as the Kinect V1 and V2 and the Structure Sensor. These three devices were among the most accessible of all the devices tested. The accuracy of the devices was assessed through the following five scanning tests: a flat surface, a platform with spheres of varying diameters, a mannequin hand,

a mannequin thigh, and a mannequin chest. The Structure Sensor emerged as the most appropriate low-cost device for orthopedic reconstruction, with an error of approximately 3 mm.

The study conducted in [37] utilizes the Structure Sensor, the Go!scan 20, and a CT machine to image 19 stomas to develop customized wafers that account for body curvature around the ostomy site. The 3D models obtained are manually cropped to the area around the stoma, and the authors decide on the outline of the stoma. The finalized model is 3D printed for the patient to use as an ostomy wafer. The patients tested wafers developed from the different scanners, and the findings suggested there were no important differences in the quality of the wafers.

Despite their utility, these external 3D scanners are typically costly and necessitate specialized training. Even the Structure Sensor—the most affordable and accurate option—remains out of reach for many patients due to its $700 price and the requirement of an iPad. However, the recent emergence of smartphones with built-in depth sensors has potential.

Our research aims to address this gap by leveraging the capabilities of smartphone-based depth sensing for the specific use case of ostomy wafer customization. In ostomy care, an accurate, user-friendly, and low-cost solution is particularly important due to the potential risks associated with improper wafer fitting. Our exploration of this application extends the potential of 3D imaging in a new direction, setting a foundation for future research in this area.

1.4 Scientific and Engineering Challenges

At the outset of this project, we hypothesized that many ostomy patients experience difficulty obtaining a properly fitting wafer, as they primarily rely on paper templates for measurement and bulky ostomy scissors for adjustment. This thesis introduces a smartphone-based system that leverages an iPhone to scan the stoma and generate its optimal contour.

A notable challenge arose from the largely unexplored domain of the iPhone's scanning functionality. Given the critical nature the application of our system, our research necessitates a thorough exploration of the specific constraints of this technology. We engage in an evaluative process of a scanning application, identifying potential issues in accuracy, usability, and other aspects that might limit the utility of the iPhone as our chosen scanning device. These limitations are documented and analyzed, providing valuable insights to inform the refining process of the application.

An associated scientific challenge lay in determining the precise location of the stoma on the 3D model and extracting a contour that could be expanded to form the optimal contour. This task requires exceptional precision, as the permissible margin of error is 2 mm. Attaining this level of accuracy presented a challenge, given the existing limitations of the scanning technology and the complexities associated with establishing a 3D workflow.

1.5 Scope of the Thesis

The scope of this thesis primarily encompasses the Osto-Mate system, as illustrated in Figure 1.3. This system integrates an iPhone application for scanning and uploading stoma scans, a database for data storage, a server that implements contour extraction algorithms, and a procedure

for translating the resultant contour into a customized patient wafer. In light of the novel use of the iPhone for scanning in this context, the thesis also investigates the device's suitability for such tasks.

Theoretical Design: The Osto-Mate system proposes a cost-effective and accessible solution by utilizing depth-sensing smartphones to capture detailed characteristics of stomas beyond what 2D imaging can provide. The system's design currently hinges on the concept of extracting contours using rules-based algorithms from 2.5D images, an approach we experiment with to minimize data needs and complexity as well as workflow requirements typically associated with 3D processing and learning-based algorithms.

Functional Design: The practical realization of the Osto-Mate system begins with developing a user-friendly scanning application tailored to suit the average stoma patient, who tends to be elderly. Given that the iPhone's scanning capabilities are not well-studied, a considerable portion of this research is dedicated to examining the device's constraints and the limitations of the adopted scanning application. Additionally, a proof-of-concept workflow is established. This explores a database service, how data is stored and accessed, server-side algorithm execution, the process of extrapolating a stoma's contour to obtain the optimal one, and the various methods available for customizing a wafer using this contour.

Future work and commercialization: As noted throughout the thesis, particularly in the discussion section, the possibility of commercializing the Osto-Mate system is considered. However, a comprehensive characterization of the iPhone's scanning capabilities is required before venturing into applications where accuracy is important. The path toward commercialization will involve optimizing the scanning and data processing aspects, ensuring patient data security and privacy, and complying with healthcare regulations.

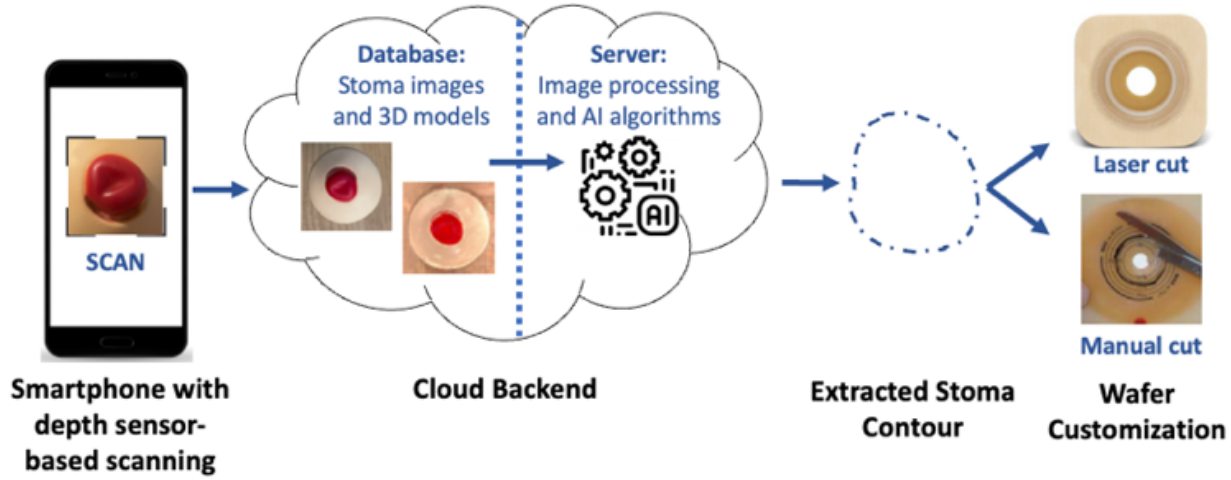

Figure 1.3: The proposed architecture of the software-based ostomy management system, illustrating the flow of data from stoma scan and image acquisition to customized wafer-cutting methods.

1.6 CONTRIBUTIONS OF THE THESIS

This thesis contributes to research in several significant ways. Firstly, it pioneers an effort to characterize the capabilities of the iPhone's TrueDepth sensor, a technological resource that holds great potential for various systems beyond our current study. Secondly, we propose a novel methodology for manipulating 3D models to extract essential features, bypassing the need for a complex 3D workflow.

The overarching contribution of this thesis lies in its advancement towards a system that leverages common smartphone technology accessible to many in the U.S. This work can serve as a valuable reference for developing similar systems in diverse fields. Most importantly, this system forms a fundamental stepping stone towards enhancing stoma care, paving the way for future research and improvements in this critical area of healthcare.

Chapter 2. METHODOLOGY

The Osto-Mate system aims to streamline the customized ostomy appliance fitting process while making it accessible to ostomates through iPhone smartphones. The system utilizes the iPhone's TrueDepth sensor to reconstruct 3D models of ostomy sites, aiming to ensure a high level of precision coupled with user-friendly operation.

The proposed system architecture is illustrated in Figure 1.3. The system comprises four primary components: 3D scanning and reconstruction, frontend user interface, contour generation algorithm, and backend server and database.

3D Scanning and reconstruction is the first part of the Osto-Mate platform and involves using the iPhone's TrueDepth sensor to capture 3D data. This sensor must be characterized to determine its accuracy and limitations. Furthermore, this system must be developed to reconstruct accurate 3D models from the captured data.

The frontend user interface is the second area of this system. This is the only section the users will interact with, so it must be designed with a focus on user experience to be intuitive and user-friendly. The interface, developed in Swift using Apple's XCode, connects with the scanning application and contour generation algorithms and allows users to view reconstruction results.

The backend server and database constitute the third area of this system. The backend of the system houses the data processing and storage components. The current prototype uses Firebase for its database and storage, with a local computer serving as the server. Future work aims to explore using Amazon Web Services (AWS) to enhance data privacy, security, regulatory compliance, and standardization.

The image processing algorithms represent the fourth area of this system. These algorithms pull data from the backend for processing. OpenCV's contour algorithms are currently employed for ostomy contour generation.

This architecture combines robust technology with a user-friendly design aimed at optimizing ostomy appliance fitting. The following sections will detail the development and testing of each component.

2.1 INTRODUCTION TO TECHNOLOGY DEVELOPED

The Osto-Mate system is a novel technology that provides accurate, user-friendly, and cost-effective 3D imaging technology for ostomy appliance fitting. Accessible via a smartphone application, this technology aims to enhance ostomy management by offering a high level of accuracy with ease of use through a readily available device and platform.

Current methods of stoma management face several challenges. These include inaccuracies in traditional methods such as template measurement, the cost and complexity of existing 3D imaging systems, and the time-consuming nature of current methods. Osto-Mate addresses these challenges by delivering high accuracy, being easy to use and cost-effective, and with the potential for additional stoma management functionality.

The innovation of our technology lies in levering the iPhone's TrueDepth sensor for 3D scanning, deploying sophisticated data processing algorithms, and creating a user-friendly interface designed with a strong focus on user experience. The research presented in this thesis is primarily dedicated to confirming the problem-solution fit, characterizing the TrueDepth sensor to ensure its suitability for medical applications, and establishing research in processing 3D data to extract relevant information.

Beyond ostomy management, the potential applications of this technology span various sectors. Beyond healthcare, it could serve as a transformative platform for industries such as retail, e-commerce, prosthetics and orthopedics, education, entertainment, tooling, and forensics. Specifically, within the healthcare sector, the system paves the way for an engaging approach to ostomy care and education, addressing an area that has long required improvement. This method could not only bolster patient engagement but also enhance providers' capability to monitor and follow up with their patients through telehealth.

2.2 Device and Smartphone Selection

2.2.1 *Selection Criteria Definition*

The following criteria are considered in the design and selection of a device whose end use is for patients to use at home and has the potential for telehealth or remote monitoring. These align with the criteria specified in [36], which are applied to scanning devices for orthopedic centers for orthoses and prostheses.

- Affordability: The device should be affordable to accommodate its intended use by a patient from home. A reasonable cost would be similar to a typical smartphone, preferably below $1000.
- Accuracy: Any device has two stages where error can be introduced: during scanning and the extraction of ostomy contours. The final error margin of the generated contour should be less than 2 mm, placing an upper bound of 2 mm on the scanning accuracy.
- Efficiency and Ease of Use: The process of scanning and any required user annotation should not take more than 5 minutes to minimize users' physical and mental effort.
- Scan Area: The device should be capable of scanning an area of at least 0.3 x 0.3 m^2. This size is sufficient for capturing the full area of most ostomy sites (Table 3).
- Mode of Operation: Given the device's intended use for at-home self-scanning by patients or assisted scanning by caregivers, the device should be handheld. This mode ensures user convenience and adaptability to various ostomy locations and patient needs.
- Compatibility and Data Security: The device should function as a standalone device to eliminate the need for additional hardware, simplifying the process for patients. Furthermore, the device must be developer-friendly so we can ensure it complies with data privacy and security laws, regulation, and standards.

2.2.2 *Exploration of Various Devices*

To develop a comprehensive list of 3D scanning devices, we included all devices characterized in the literature [36, 38-41] as well as current devices on the market. We selected the latter based on their popularity and affordability, with a price point of less than $2,000 [42-44]. The devices are summarized in Table 1.

Table 1
Overview of 3D Scanning Devices Characterized in Literature and Current Market.

Device	Device Image*	Technology	Acquisition Range (m)	Accuracy (mm)	Connectivity, Scan Manner	Cost
Artec Leo		White Structured Light [36]	0.35 – 1.2 [36]	0.1 [36]	Wireless, Handheld [44]	$32,300 [44]
Artec Spider		Structured light / Speckle Pattern [39]	0.17 – 0.35 [39]	~0.05 [39]	USB, Handheld [44]	$23,800 [44]
ASUS Xtion		Infrared Pattern Triangulation [45, 46]	0.8 – 3.5 [46]	N/A	USB, Handheld & Table [46]	$300 [46]
Creaform HandySCAN 700		Stereo photogrammetry [39]	0.3 – 4 [39]	0.2 + 0.06 per m [39]	, Handheld & Table [39]	$19,500 [47]
Creality CR-Scan 01		Structured Light [44]	0.3 – 0.5 [48]	0.5 [48]	USB, Handheld & Table [48]	$554 [44]
Creality CR-Scan Ferret		N/A	0.15 – 0.7 [49]	0.1 [43, 49]	USB, Handheld & Table [49]	$349 [49]

FreeScan X7		Stereo photogrammetry [39]	0.10 - 8 [39]	0.02 + 0.06 per m [39]	USB, Handheld [50]	N/A
GOM ATOS II 400		Black and White Fringe Pattern Triangulation [36]	N/A	N/A	Computer, Table [51]	$19,250 [51]
Intel RealSense D435		Stereoscopic [52]	0.3 – 3 [52]	<2% at 2 m [52]	USB, Handheld & Table	$314 [52]
iPhone		Infrared Pattern Triangulation [53]	N/A	N/A	Wireless, Handheld	$629 (for iPhone 12) [54]
Kinect V1		Infrared Pattern Triangulation [36]	0.5 – 6 [36]	N/A	USB w/ Adaptor, Handheld & Table	$20 (used)
Kinect V2		Infrared Time of Flight [36]	0.4 – 5 [36]	N/A	USB w/ Adaptor, Handheld & Table	$20 (used)
Konica Minolta Vivid 9i		Laser Triangulation [36]	0.5 – 2.5 [36]	0.1 – 0.2 [36]	SCSI, Table [55]	N/A
Mantis PocketScan 3D		Structured light / Speckle Pattern [39]	0.25 – 1.00 [39]	2 at 1m [39]	N/A	N/A
Matter and Form 3D Scanner V2		Laser Triangulation [44]	N/A	0.1 [43]	USB, Table [43]	$749 [44]

NextEngine Ultra HD		Laser Triangulation [36]	0.19 – 0.71 [36]	0.13 [36]	USB, Table	N/A
Phiz 3D Scanner		Laser Triangulation [56]	N/A	0.2 [56]	Wireless, Table [56]	$379 [56]
Prime Sense		Infrared Pattern Triangulation [45]	0.35 – 3 [45]	1[45]	USB, Handheld & Table [45]	$295 [45]
Revopoint POP 2		Structured Light [42]	0.15 – 0.4 [42]	0.05 [42]	USB, Handheld & Table [42]	$699 [42]
Rodin4D O&P Scan		Laser Triangulation [36]	0.05 – 0.3 [36]	0.5 [36]	USB [57], Handheld [36]	$10,000 [36]
Scan Dimension Sol		Laser Triangulation [44]	N/A	0.1 [44]	USB, Table [56]	$799 [44]
Sense 3D Scanner 2nd Gen		Stereoscopic [58]	< ~1	1 [58]	USB, Handheld	$300 [58]
Shining 3D EinScan-SP		Structured Light [42]	0.29 – 0.48 [42]	0.05 [42]	USB, Table [42]	$2,100 [42]

Shining 3D Einstar		Structured Light [42]	0.16 – 1.4 [42]	0.1 [59]	USB, Handheld [42]	$959 [42]
Structure Sensor Pro		Infrared Pattern Triangulation [36]	0.3 – 5 [36, 60]	~4 [36]	Tablet, Handheld [60]	$995 [60]

Note: *Device images are sourced from [36, 38, 39, 41-44, 54, 57, 58, 61].

2.2.3 *Comparison and Decision Making*

To streamline the selection of devices from Table 1, we initiated a process of elimination based on the constraints specified in section 2.2.1. The devices were eliminated for the following reasons:

- Discontinuation: FreeScan X7, Konica Minolta Vivid 9i, Mantis PocketScan 3D, NextEngine Ultra HD.
- Cost considerations (beyond the affordability range): Artec Leo, Artec Spider, Creaform HandySCAN 700, GOM ATOS II 400, Rodin4D O&P Scan, Shining 3D EinScan-SP
- Compatibility issues: ASUS Xtion, Creality CR-Scan 01, Creality CR-Scan Ferret, Intel RealSense D435, Kinect V1, Kinect V2, Matter and Form 3D Scanner V2, Prime Sense, Revopoint POP 2, Rodin4D O&P Scan, Shining 3D Einstar, Scan Dimension Sol, Sense 3D Scanner 2nd Gen.
- Mode of operation: Phiz 3D Scanner

Following this process, the devices that met all the criteria were the Structure Sensor Pro and iPhones. The combability constraint removed many options, largely due to our strict requirement for devices to be standalone. Although there is a potential opportunity to use the sensors within some of the more affordable options, such as Intel RealSense D435, Kinect V1, Kinect V2, and Prime Sense, to create a standalone scanning device, we decided to focus our efforts on utilizing pre-existing, fully integrated devices.

2.2.4 *Justification for Selecting the iPhone*

The final contenders for our scanning device are the Structure Sensor Pro and iPhones. While the Structure Sensor Pro nears the end of the affordability range and might be affordable for certain caregiving agencies, it is impractical for a patient to purchase or rent a tablet along with the device and scan their own ostomy. This setup might be plausible for home health or nursing home scenarios, but it would likely be too costly for home health agencies to consider.

The iPhone, on the other hand, presents a compelling alternative. Its widespread adoption, with 48.7% of smartphone users in the U.S. owning an iPhone [62], alongside its accessibility and convenience, makes it a fitting platform for the customization of ostomy appliances and

general ostomy management. However, its potential in this area is largely unproven and requires further research.

Other smartphones with specialized scanning sensors are available on the market [63], but none demonstrate consistency across all their models as iPhones do. Research into 3D reconstruction via smartphones, aside from photogrammetry techniques, is largely unexplored. A search conducted on IEEE Xplore, using the keywords "iPhone" AND "scan," as well as "true depth" in separate queries, yields a total of 14 publications. Notably, only two of these delve into the precision of iPhone scanning via applications in the app store, indicating a significant gap in the research landscape. Nevertheless, the consistency of iPhones, specifically the inclusion of the TrueDepth sensor across all recent models, makes it an ideal platform for our technology. It provides the potential to make our technology widely accessible using a device many people already own.

2.2.5 *Specifications of the Selected iPhone*

With our decision to use the iPhone as the platform for the Osto-Mate system, it's crucial to understand the specifications and potential limitations of the device (Table 2). The specific model used in our research is the iPhone 12, which is capable of estimating over 30,000 depth points [64]. Within an optimal scanning range of 25 to 50 cm [65], the device is expected to sample 0.42 to 0.1 points per mm^2. It is essential for our research to verify whether this density is sufficient to create custom wafers within an acceptable margin of error consistently.

Our tests, using the infinitam_ios application [66], demonstrate the iPhone's capacity to sample depth at a frequency of 30 Hz. A high sampling rate is vital as it affects the granularity and precision of generated 3D models. High-frequency sampling enables the model to capture more detailed changes and potentially reduce the error introduced in registration from sudden movements.

Moreover, the iPhone's front-facing camera, possessing a 12-megapixel resolution and a 120-degree field of view [54], will be used to incorporate color into the models. These camera specifications help to determine the quality and range of the color data that will be overlaid onto the 3D model. High resolution and a wide field of view can enhance the visual quality of the model, making the stoma easier to visualize and understand.

Although we currently do not anticipate employing video recordings to develop the model, we have included the video recording specifications of the iPhone 12. The extensive video capabilities may present additional options for future development and enhancements of the Osto-Mate system.

Table 2
Key Specifications of the iPhone 12

Specification	**Available on devices used**
Number of depth points sampled	30,000+ [64]
Optimal scanning distance	25 cm to 50 cm from object [65]

Estimated depth points per mm^2 in optimal scanning distance	0.42 to 0.1
Frequency of depth points sampled	30 Hz
Camera	12-megapixel camera with an aperture of f/2.2 and a field of view of 120 degrees [54]
Video recording	The imaging system's camera has the following recording specifications [54]: ● HDR video recording with Dolby Vision up to 4K at 30 fps ● 4K video recording at 24 fps, 25 fps, 30 fps, or 60 fps ● 1080p HD video recording at 25 fps, 30 fps, or 60 fps

2.3 CHARACTERIZING THE SMARTPHONE FOR 3D RECONSTRUCTION

2.3.1 *Preliminary 3D Scanning Experiments*

In the preliminary scanning phase of this research, we evaluated the potential of the iPhone 12 as a scanning device for 3D ostomy reconstruction. The iPhone 12 is equipped with a TrueDepth camera system, which is particularly known for enabling Face-ID functionality. This system incorporates a near-infrared projector and collector, facilitating depth measurements similar to the operations of the Kinect V1 [67]. Our findings indicated that the iPhone's depth imaging system has an accuracy of over 2 mm on average with smaller-sized objects. This level of accuracy is expected to be consistent across other iPhone models that are also equipped with the Face-ID capability.

This section details the preliminary process that was taken to determine the accuracy of the iPhone's scanning system. Basic objects were scanned using the iPhone and the NextEngine 3D Scanner Ultra HD and compared to evaluate the iPhone's accuracy.

2.3.1.1 Reference 3D Scanner

The NextEngine 3D Scanner was used as a reference due to its demonstrated sub-millimeter accuracy in [36]. The NextEngine 3D Scanner uses various lasers in conjunction with a single-axis turntable to capture an object's varying surfaces through a series of scans. Following the initial scan, any missed angles or surfaces can be captured by manually adjusting the object's position and conducting additional scans. These subsequent scan series are roughly aligned and then precisely merged by the ScanStudio software to develop the final 3D model.

2.3.1.2 Assessment of the iPhone's TrueDepth Camera System

The iPhone's TrueDepth sensor, known for its role in Face-ID recognition, was evaluated through the publicly available Infinitam_ios application [66]. This application constructs monochrome STL models in real-time by combining the depth and image data from the TrueDepth and camera sensors. Efforts to utilize the iPhone's LiDAR sensor were thwarted due to its sparse array, making it less suitable for detailed 3D reconstruction [67].

2.3.1.3 Comparative Model Evaluation

The iPhone's accuracy was evaluated by comparing its produced 3D models of geometrically simple objects and a stoma model (Table 3), mirroring the approaches taken by previous works [30, 36]. The comparison involved three methods: a visual analysis of the absolute distance errors in the iPhone-generated models via annotated heatmaps, generation of cumulative distribution graphs for distance errors, and computation of mesh-to-cloud mean distance error and standard deviation. All model comparisons were done using the CloudCompare software.

Table 3

Measurements and Geometries of Simple Objects

Objects:	Cube 1	Cube 2	Rectangle 1	Rectangle 2
Measured Dimensions:	11.9 mm length, width, height	16.1 mm length, width, height	32.1 mm length, 16.2 mm width, 6.0 mm height	48.0 mm length, 16.3 mm width, 9.1 mm height
Object Image:				

Table 3 Continued

Measurements and Geometries of Simple Objects

Objects:	Cylinder 1	Cylinder 2	Half-Sphere 1	Half-Sphere 2	Stoma model
Measured Dimensions:	5.1 mm height, 13.7 mm diameter	15.0 mm height, 25.7 mm diameter	17.3 mm height, 36.1 mm diameter	23.3 mm height, 50.1 mm diameter	75.9 mm skin diameter ~ 30 mm red spout diameter

Object Image:					

2.3.1.4 Experimental Setup and Calibration

The objects were fixed onto a marked cardboard surface and positioned on a single-axis turntable about 241mm from the NextEngine scanner. The models produced by the NextEngine scanner are scaled in CloudCompare using the marking to equate 1 unit distance with 1mm.
For the iPhone scans, the objects were placed on a flat surface, and the iPhone was held approximately 220mm above the surface. The iPhone was manually maneuvered over the object to ensure comprehensive model reconstruction. A small half-sphere object of known diameter was used to determine the scale factor for the iPhone's produced models. To compare the test and reference 3D models, the test model was scaled, manually aligned through rotation and translation, cropped to remove background, and finely aligned to the reference model CloudCompare's iterative closest point algorithm.

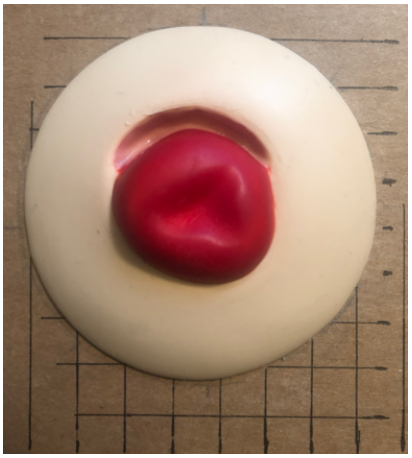

Figure 2.1: Depiction of the stoma model secured onto a cardboard surface, marked with 10 mm intervals between lines.

2.4 DEVELOPMENT OF THE SYSTEM

2.4.1 *Frontend*

This section outlines the frontend user interface of our iOS application, designed specifically for ostomy patients to scan their stomas, extract outlines, and order customized wafers. We will note that the application displayed in this section is largely a mockup.

Upon first interaction, the user is greeted by a clean interface imbued with baby blue, a color often associated with calmness and frequently used in logos of companies [68]. The application utilizes either Calibri or Arial fonts, known for their readability, with large font sizes for user

convenience. The layout follows a minimalist design, with each screen serving a single purpose, thereby simplifying navigation and minimizing potential confusion. For example, the main page merely lists the available options (Figure 2.2 (c)), unlike more complex applications that often feature numerous icons on the top and bottom bars.

We have deliberately streamlined the process to minimize mental and physical effort. At its most efficient, ordering requires a mere nine clicks: five to extract the outline and specify the quantity and four more to place the order. Given saved data, the ordering process can take less than a few minutes, depending on the stoma's complexity which affects the scanning duration. We estimate the typical stoma scan takes under 10 seconds, making the overall process swift and efficient.

Upon launching the application, the user encounters the login in page, displayed in Figure 2.2 (b), offering standard options to log in, create an account, or retrieve forgotten information. In the interest of simplifying usage for elderly patients, we are considering the implementation of Face ID to reduce the effort required to use our application. However, additional research is needed to determine patient data security laws around this.

Once logged in, the user is directed to the main page featuring the application's primary functions: "Scan and Order," "Order History," "Stoma History," "Settings," and "Help." Each function is represented by a large, clearly labeled button. The primary function, "Scan and Order," is strategically positioned at the top.

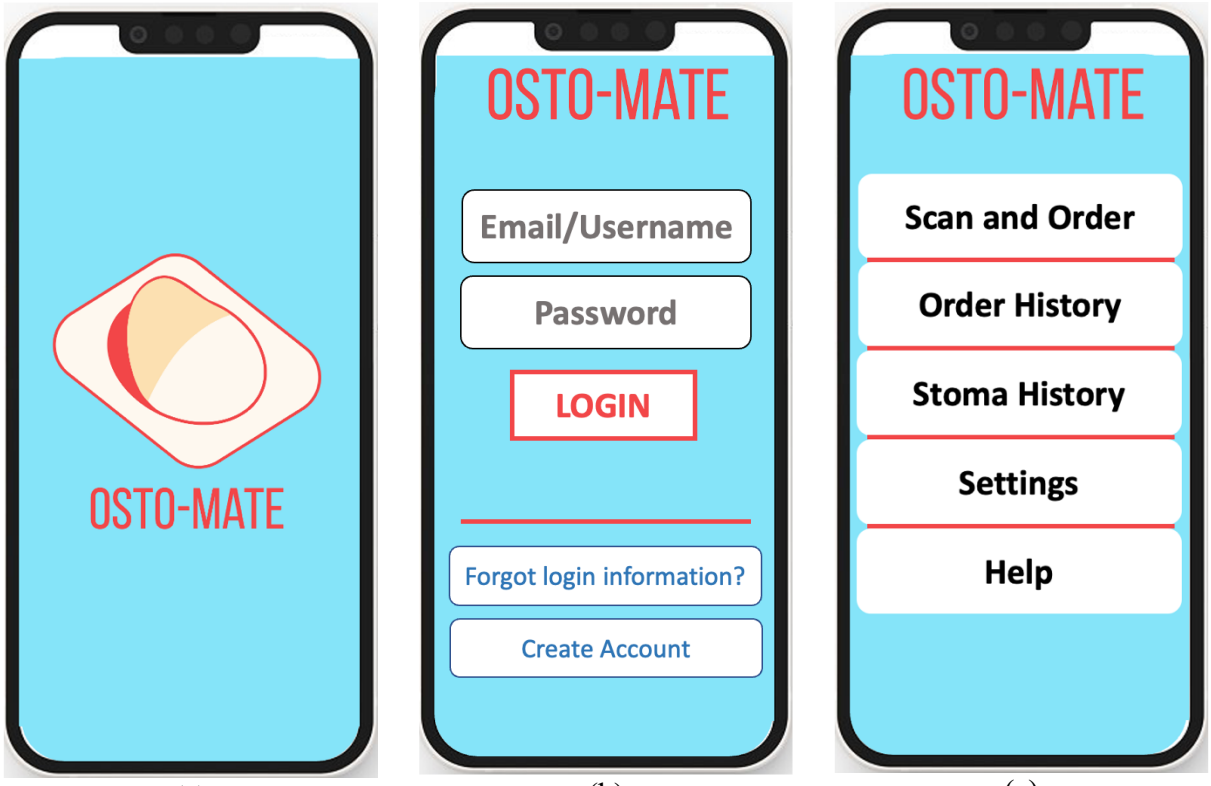

(a) (b) (c)

Figure 2.2: Initial User Interface Screens of the Application. The images demonstrate the launch screen (a), login screen (b), and main screen (c).

When the user selects "Scan and Order," they are directed to the pre-scanning guidance page (Figure 2.3 (a)), adapted from the infinitam_ios application [66]. This screen provides a simple visual guide, indicating whether the phone is positioned correctly for scanning: green indicates optimal scanning distance, and orange-red means the phone should be brought closer to an object if that is the object of interest. After properly positioning the phone, the user initiates the scan by clicking the large "Scan" button (Figure 2.3 (b)), subsequently creating a 3D model of the stoma. The scan will display a gray model with gaps where the model is incomplete, which the user must attempt to fill by moving the phone around. Once the model appears complete, the user will press "Create Model" to bring up a finalized model with the extracted outline superimposed for confirmation. Future iterations may allow the user to fine-tune the outline, but caution must be taken to balance functionality and usability, as working in 3D with a touchscreen can become easily sophisticated. Another option under consideration is a "Flag Extracted Outline" feature, enabling a nurse to review and manually adjust the outline, subject to user confirmation.

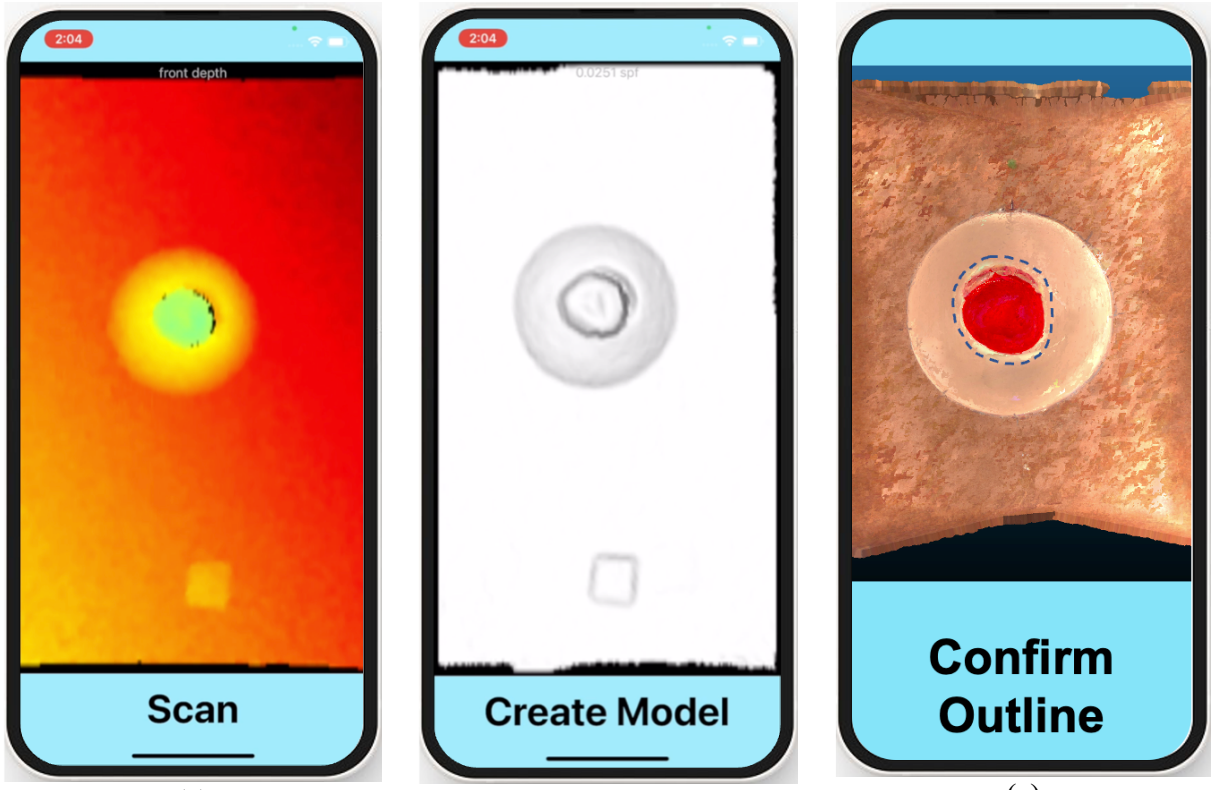

(a) (b) (c)

Figure 2.3: Overview of the User Interface Screens during the Scanning Process. The sequence begins with the pre-scanning guidance screen (a), transitioning to the active scanning screen (b), and concluding with the outline confirmation screen (c).

Upon approving the outline, the user is led to the order page (Figure 2.4 (a)), where they can select their preferred wafer(s) and specify the quantity. Once the wafer type and quantity are determined, the user proceeds to the delivery page, where the pre-stored is used by default to minimize input requirements. At this stage, the users can choose between standard and expedited shipping options. The process concludes with the payment information page, where we hope to integrate existing reimbursement options from Medicare and private insurance. For those paying out of pocket, the user can add another payment option. Once all the details are confirmed, the user will end at a summary page that displays their order and the cost, and the user can submit the order.

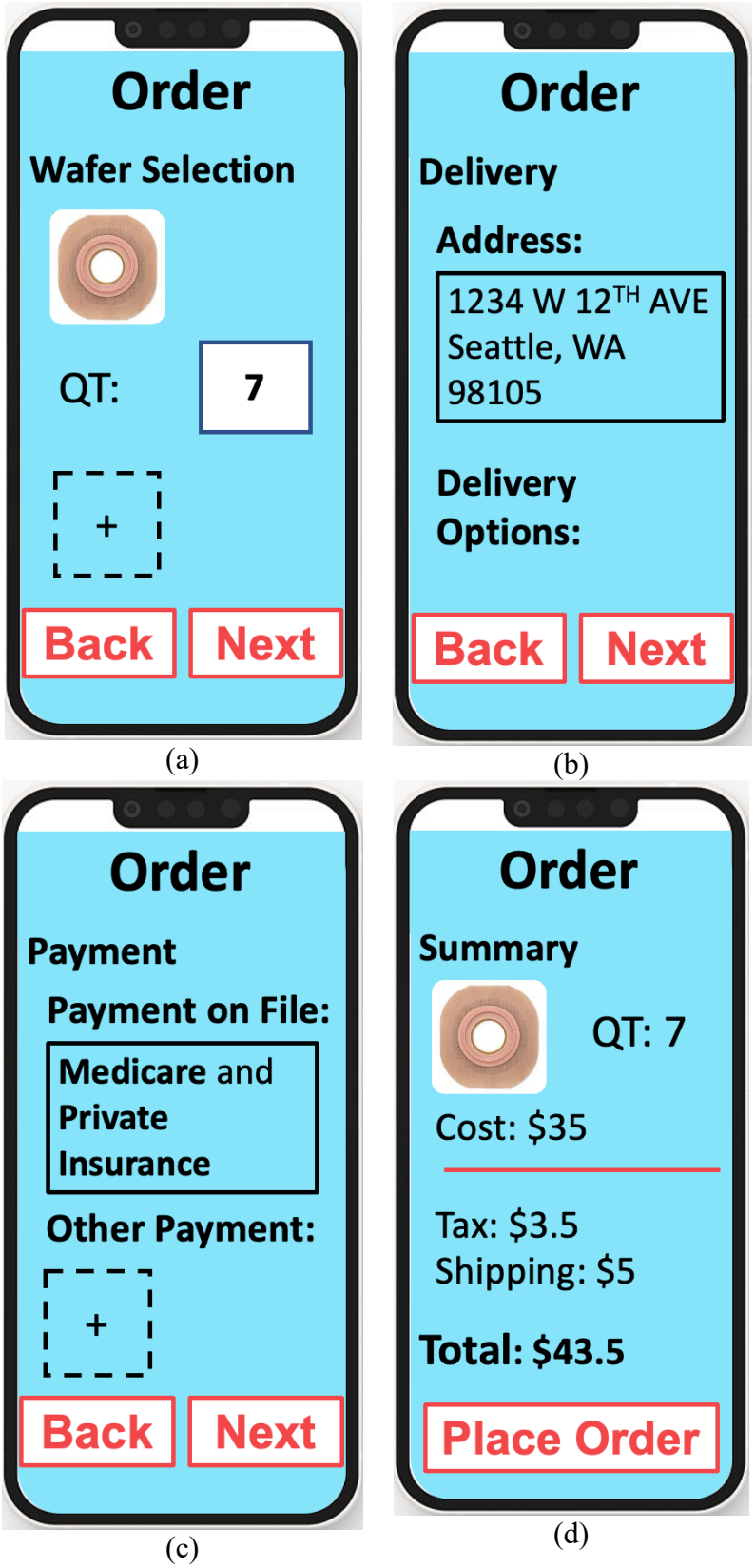

Figure 2.4: Sequence of User Interface Screens for the Ordering Process. The images display the wafer selection

screen (a), followed by the delivery details screen (b), payment information screen (c), and culminating with the order summary and final purchase confirmation screen (d).

From the main screen, users have access to view their "Order History." This feature offers an organized look at the user's previous orders, starting with the most recent at the top. Each order displays a comprehensive summary, including images of the ordered items, quantities, and current delivery status. Users can easily scroll through their order history for a quick review or more in-depth information. For instance, as depicted in Figure 2.5 (a), selecting the order from August 1st brings up a detailed summary of that particular transaction (Figure 2.5 (b)).

(a) (b)

Figure 2.5: Review of User Interface Screens for Order History. The images present the main Order History screen (a) and the detailed summary view of a selected previous order (b).

Another accessible feature from the main screen is the "Scan History." This feature organizes and displays all past stoma scans from associated wafer orders in a scrollable list. Selecting any of these past scans leads the user to a screen presenting an image of the extracted stoma outline with a measurement of the longest length for reference. Furthermore, the application offers an interactive element to these images; a swipe to the left displays the contour overlayed on an image of the stoma captured during the scanning process. An additional left swipe provides an even more immersive experience, revealing a fully interactive 3D model of the stoma with the outline

superimposed. Navigational cues, represented by three circles beneath the images, indicate the total number of images and the user's current position within this sequence.

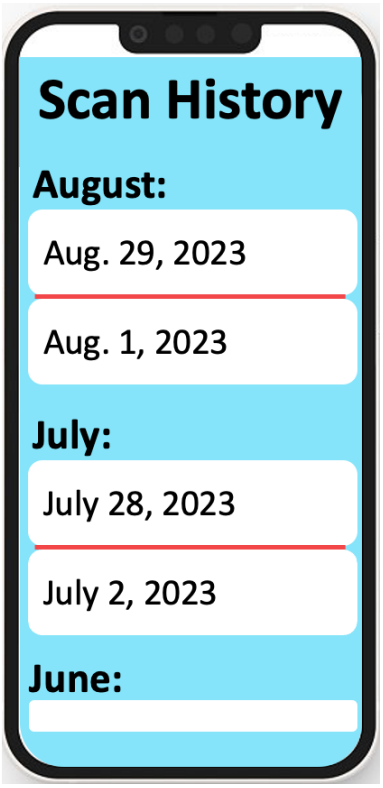

(a)

(b)

(c) (d)

Figure 2.6: User Interface Screens of Scan History. The sequence displays the primary Scan History screen (a), followed by a detailed view of a selected past scan showcasing the custom wafer outline (b). Further interaction reveals the overlay of the custom outline on an actual image of the user's stoma (c) and the outline superimposed on an interactive 3D model of the stoma (d).

The application's two other functions include "Settings" and "Help." The "Settings" options enable users to adjust account details and preferences. Account details include preferred payment methods, default delivery address, and other user information, while preferences in future iterations would allow the user to select from different aesthetic layouts, fonts, and font sizes. The "Help" page provides user guides, ostomy maintenance tips, FAQs, and a yet-to-be-determined technical support button.

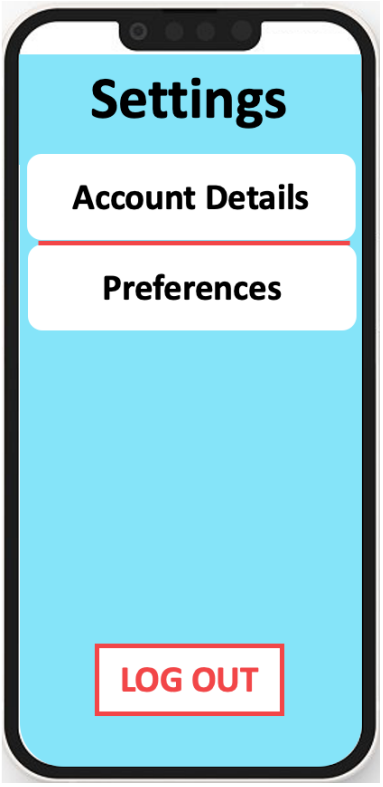

Figure 2.7: User Interface of the Settings screen.

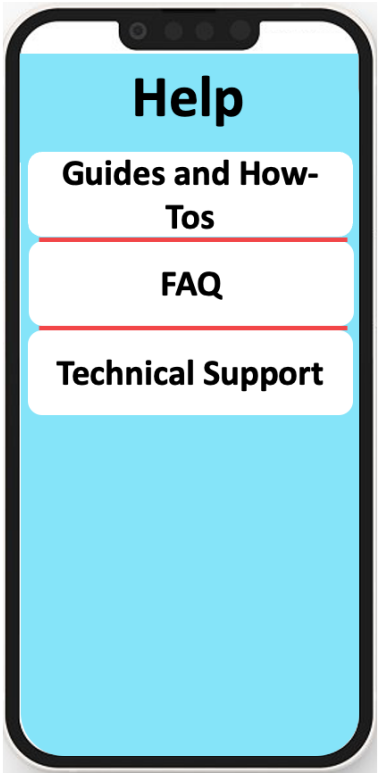

Figure 2.8: User Interface of the Help screen.

The application shown in the figures for this section is largely a mockup, but it will be developed using Swift, Objective-C, and XCode for iPhone users due to our system's technological compatibility. The stoma scan is processed in Python once uploaded to our server and database, with a potential future transition to C/C++ for faster 3D model processing.

While the initial application is primarily a tool for facilitating the scanning and ordering process, we envision future versions supporting community interaction among ostomy patients and enabling users to share scanning data with their providers. This initial version, however, is tailored to be as intuitive and simple as possible, potentially allowing users to complete the ordering process in under a minute.

2.4.2 *Scanning*

The scanning functionality of our application is adapted from [66], which integrates the Infinitam framework [69] with iPhones to reconstruct 3D objects. This application, freely available under the Oxford license for research purposes, serves as the foundation for our preliminary stage implementation. Our adapted scanning process is outlined in Figure 2.9.

As detailed in the previous section, the pre-scanning screen (Figure 2.9 (a)) offers guidance for users to determine the optimal scanning distance. Once the iPhone is appropriately positioned, the user initiates the scanning process. A grayscale 3D model begins to form on the screen, with the user aiming to fill as many of the gaps in the model as possible by maneuvering the iPhone. After achieving sufficient model coverage, the user selects "Create Model." As currently implemented, the application then displays the extracted 3D model, which can be interacted with via zooming,

translating, and rotating. Upon approval of the model, the user selects “Upload Model” near the top of the screen (Figure 2.9 (c)). Once the model is uploaded, the users receive either an “Upload Successful” or “Upload Failed” message (Figure 2.9 (e)).

We will delve into the challenges associated with this application, particularly regarding the scanning aspects, in the results section. Broadly, the scanning application struggles with accurately rendering tall or symmetrical objects. Furthermore, it does not do well in capturing finer details or smaller objects due to issues with tessellation and lack of color representation. Future improvement efforts should begin with a more detailed characterization of the TrueDepth sensor using raw scanning data, if possible, to understand the iPhone’s constraints better.

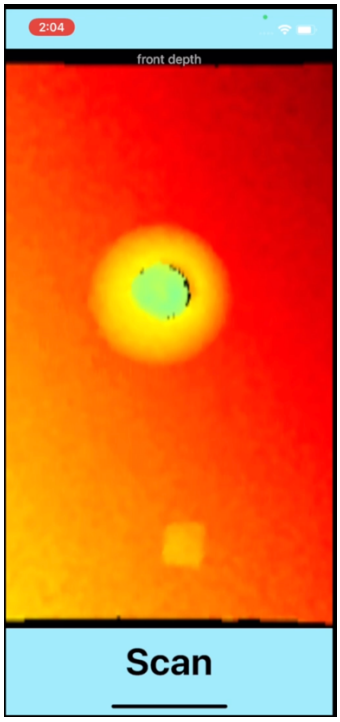

(a)

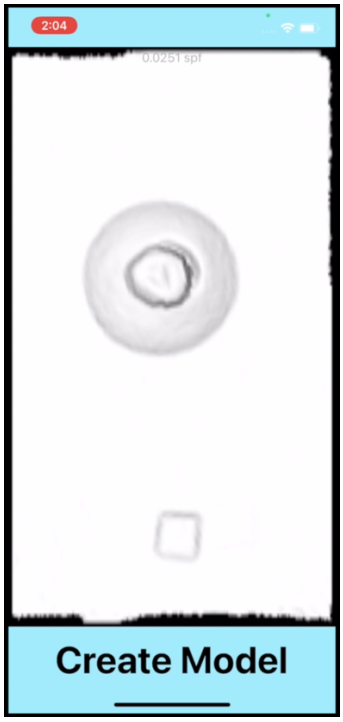

(b)

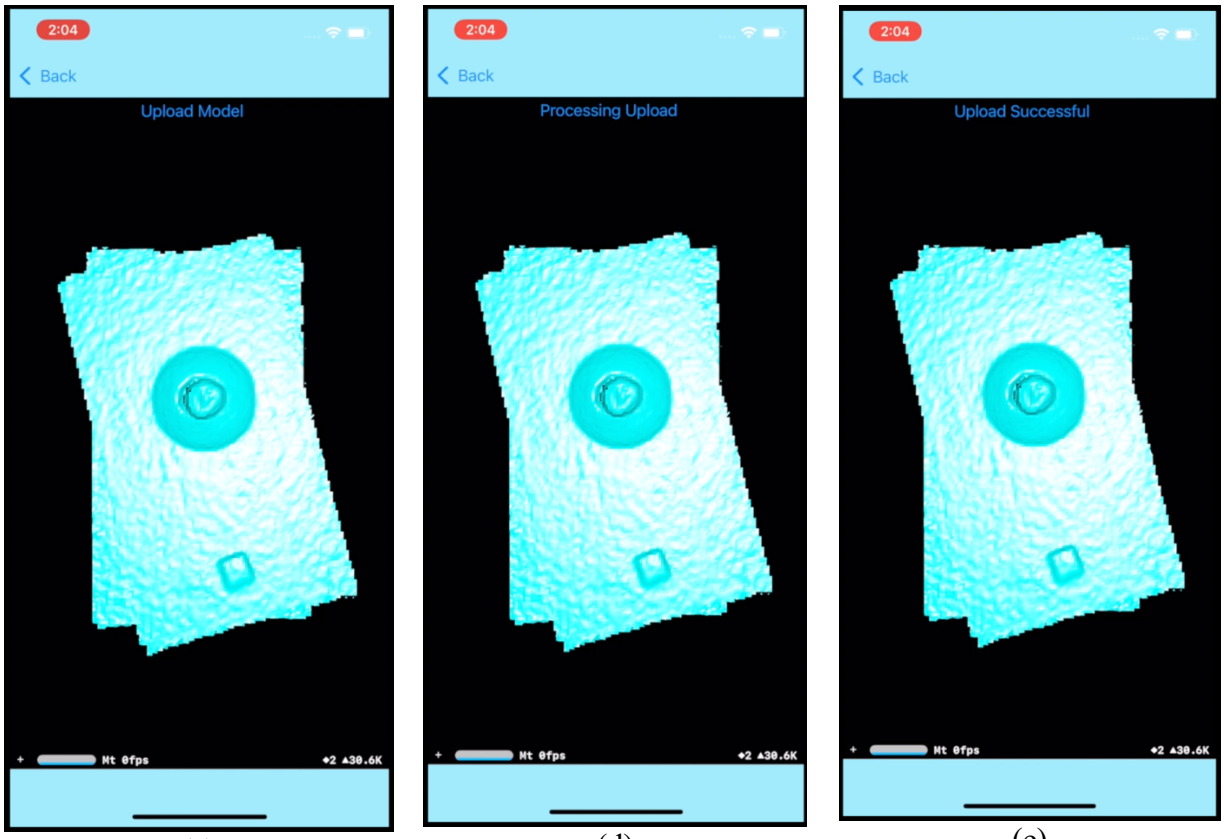

(c) (d) (e)

Figure 2.9: Current Scanning Process in the Osto-Mate Application.

2.4.3 *Backend*

Although processing an ostomy patient's scan locally on the patient's iPhone might seem feasible, factors like computational speed, data security, and potential future integration with healthcare institutions' electronic medical records sway us towards a database and server configuration. For our initial system, we utilize Firebase's Database and Storage, chosen primarily for their simplicity and multi-language support for setup and data manipulation.

When a user opts to upload a scan, the model is uploaded to Firebase's Storage using Swift code, which Firebase's documentation details [70]. After the 3D model is uploaded, we obtain the URL where the scan is stored. This URL, alongside the scan's name, is subsequently uploaded to Firebase's Database. Notably, Firebase's Database and Storage function independently—the database only accommodates text, while the storage is designed for images and other file types. When a scan is ready for processing, the "scan_start" variable is set to 1, enabling a server to identify all uploaded but unprocessed scans.

In this prototype system, our server is a local computer set to check for unprocessed scans every second. Upload locating one, it downloads the 3D model, runs the contour generation algorithm, and uploads the contour's point set as an image. While this serves as a placeholder

format at present, the final outline file format is pending finalization. After the file is uploaded to Storage, the URL is uploaded to the Database, and the "scan_done" variable is set to 1.

Designed initially for use by a single testing device with non-patient data, this system is scalable, although it will require establishing user authentication and authorization, as well as adherence to regulatory laws. Utilizing a 2017 MacBook Air as the server, the current system can typically process a scan in less than five minutes. With a view to potentially processing thousands of scans, algorithm optimization for multi-threaded execution will be needed, especially when a server service is used. This initial configuration is solely for proof of concept and will not be used for handling actual patient data. Future versions will prioritize data privacy, security, and field-specific standards, such as FHIR 7, as well as seamless integration with existing healthcare systems, aspects that require further research.

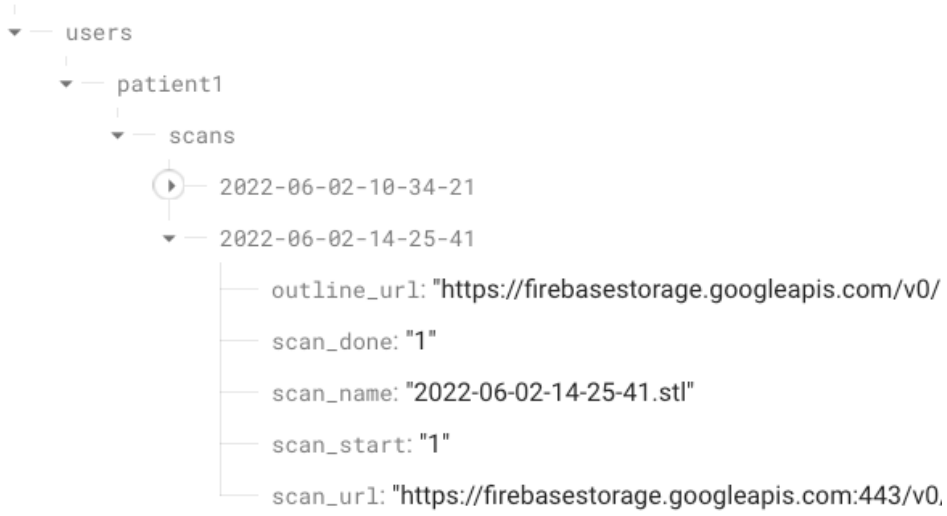

Figure 2.10: Firebase Database Data Hierarchy.

2.4.4 *Contour Generation Algorithm*

Continuing our exploration of this technology's potential, we conducted scans on fifteen different stoma models using the iPhone. For the contour extraction, we applied Suzuki's rules-based contour algorithm on 2.5D images [71], a widely recognized method in the OpenCV library used for image processing. The goal of this step was to assess if the topological characteristics of stomas could enable a simple and reliable extraction. This could help avoid the necessity for complex 3D object detection algorithms, which usually require large datasets and a sophisticated workflow. Preliminary observations suggest that rules-based algorithms might not provide robustness or stability for comprehensive stoma management due to the stoma's intricate geometry and color variation.

In the sections to follow, we will delve deeper into our stoma outline extraction methodology, explore the potential limitations of smartphone-based 3D scanning for stoma contouring, and analyze the errors associated with Suzuki's contour [71].

2.4.4.1 Data Collection

As an attempt to reflect the actual diversity encountered in clinical scenarios, we based our methodology on fifteen distinct stoma models (Table 4), obtained from [72]. These models represent only a fraction of possible variations in color, size, and environment surrounding stomas.

In this effort, we focus on extracting the exact contour of the stoma to simplify the contour expansion process; typically, the stoma outline is expanded with a margin of one-fourth to one-eight of an inch, but the process of expanding the extracted contour itself may lead to errors, so we will propose a preliminary option that will need to be explored as future work. The stoma contour is ideally extracted from an overhead view—a process that currently relies on trial and error and best judgment. For generating a reference contour in our study, we positioned the models on a flat cardboard surface marked with a checkered pattern. This facilitated image alignment and scaling. We used the iPhone 12's back camera to photograph the stoma models. To mitigate perspective distortion, we secured the iPhone on a platform, ensuring it was parallel to the surface on which the stoma was placed (within 1 degree in the X and Y direction).

Aligning with the system shown in Figure 1.3, first, the stomas were scanned using the iPhone 12 with the scanning methodology described in Figure 2.9. To enable an accurate comparison between the extracted contour and the reference contour, we maintained the stoma's orientation by scanning it after capturing the initial image. The process yielded monochrome 3D models, as demonstrated in Figures 2 (a) and (b). We processed the generated 3D models using CloudCompare to 1) scale the model such that a unit aligns with millimeters, 2) crop to only include the stoma and cardboard surface, 3) level so that the cardboard surface coincides with the X-Y plane, and 4) align the model to match the orientation of the cardboard in the reference images.

Table 4

Stoma Models Description and Images

ID	S1	S2	S3	S4	S5
Description	Stoma with a mucatenous separation	Recessed stoma	Flush stoma with nearby hernia	Flush stoma	Stoma located within a body crease
Image	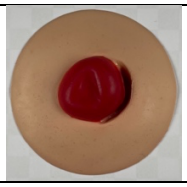	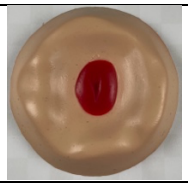	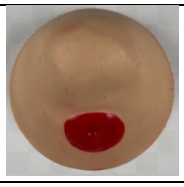	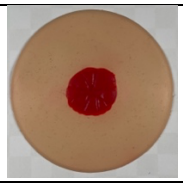	
Dimensions (Major Axis x Minor Axis x Height)	29 mm x 27 mm x 12 mm	24 mm x 18 mm x 2 mm	25 mm x 20 mm x 2 mm	24 mm x 21 mm x 1 mm	21 mm x 17 mm x 1 mm

Table 4 Continued

Stoma Models Description and Images

ID	S6	S7	S8	S9	S10
Description	3” diameter stoma	Granuloma stoma	Mushroom stoma	Double barrel stoma	Prolapsed stoma
Image					
Dimensions (Major Axis x Minor Axis x Height)	67 mm x 65 mm x 38 mm	27 mm x 24 mm x 13 mm	27 mm x 27 mm x 21 mm	64 mm x 33 mm x 11 mm	31 mm x 28 mm x 51 mm

Table 4 Continued

Stoma Models Description and Images

ID	S11	S12	S13	S14	S15
Description	2” diameter stoma	7/8” diameter stoma	Ischemic stoma	Oval stoma	Loop stoma
Image					
Dimensions (Major Axis x Minor Axis x Height)	49 mm x 47 mm x 21 mm	23 mm x 22 mm x 13 mm	49 mm x 47 mm x 20 mm	29 mm x 23 mm x 10 mm	47 mm x 28 mm x 16 mm

2.4.4.2 Ground Truth Contour Extraction

Before we undertook any processing, we noted that minor shifts of the stoma and cardboard background from image to image and scan to scan could lead to alignment inaccuracies between the ground truth contours and the extracted contours. To minimize alignment discrepancies from the outset, we selected a representative pair (one ground truth image and one 2.5D image derived

from the 3D model). We based our selection on the clarity of the cardboard edges delineated in the 3D model, which aided alignment. We visually aligned this pair using the overall shape of the cardboard surface. Despite the potential for slight error introduction through this method, we employed further alignment of the extracted contours to offset these errors, which we will elaborate on later.

Once we had aligned the pair, we matched all other ground truth images to the selected ground truth images and aligned all 3D models to the chosen 3D model. This method was a necessity due to the challenges posed by tessellation and the absence of color in the 3D models, which hampered direct objective alignment between each pair of ground truth images and 3D models with registration algorithms like SIFT and TurboReg in Fiji.

To align the ground truth images, we first cropped the images to the edges of the cardboard surface and then used the Scale-Invariant Feature Transform (SIFT) algorithm within Fiji for precision alignment. This algorithm selects key features within the images and calculates the optimal rotations and translations for alignment. These transformations maintain the final contour's integrity, as they avoid alternations such as scaling. Though this alignment is not directly observable, it was applied to the images shown in the 'Ground Truth Contours' column of Table II. We aligned the 3D models in a similar fashion, manually applying translation and rotation transformations.

The ground truth contours extraction process from the images involved: 1) applying color thresholding to emphasize the shape of the stoma, 2) transforming the image to a binary mask, 3) removing any background objects, 3) filling in the holes present in the stoma's mask, and 4) manual correcting any inconsistencies in the stoma's mask by overlaying the mask onto the original stoma image. The mask's outer set of pixels then yielded the ground truth contour. The error from manual correction did not exceed 0.15 mm from the optimal contour at any given point.

2.4.4.3 Contour Extraction

Our aim was to reduce the complexity involved in analyzing 3D models by concentrating on the stoma's topography with 2.5D images, which can be examined with 2D imaging techniques. To produce these 2.5D images from the 3D models, first, a height gradient was applied, which maps the range of Z values (or height) in the model to a spectrum, thus demonstrating the topography of the 3D model. As stated earlier, we leveled the model so that the X-Y place corresponds to the surface on which the stoma is placed. As a result, any color variations on the model correspond to differences in height.

In our procedure, we applied a grayscale gradient with a gray-white-gray spectrum, with the lowest points as gray, mid-range as white, and highest points as gray, using the Python library vtkplotlib (Figure 2.11). The 2.5D image was obtained by screenshotting this model from an overhead perspective. The 2.5D image's scale was established by comparing the XY distance of two identifiable points on the 3D model to those on the 2.5D image. These 2.5D images were subsequently resized to match the scale of the ground truth images.

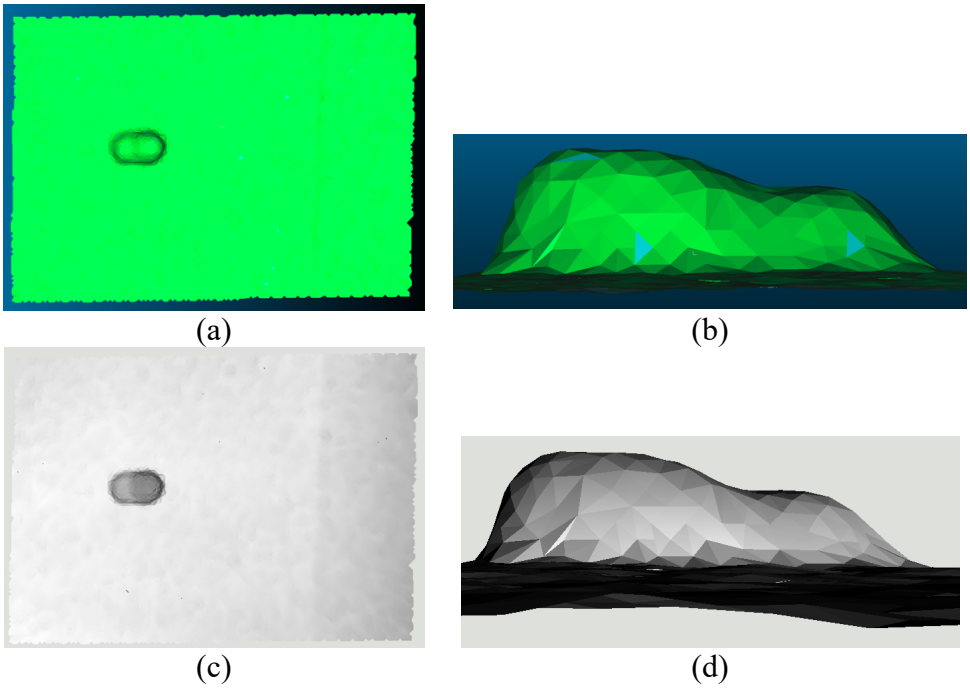

Figure 2.11: Illustration of the applied height gradient. Images (a) and (b) show the original stoma model viewed from overhead and side perspectives, respectively. As the stoma model is in STL format, it does not inherently display color. Therefore, the CloudCompare software applies a default color scheme of green and blue with shading to the model for visualization. Following the height gradient application, the altered stoma model is depicted from overhead in image (c) and from a side view in image (d).

Before delving into the specific methodology for extracting the stoma's contour, it is essential to provide some context on the general process of contour identification. Our approach uses OpenCV via Python for contour extraction from the images [73]. The initial step is to convert the image to grayscale (Figure 2.12 (a)), followed by thresholding. Here, we apply binary thresholding with the threshold value determined by Otsu's method, an algorithm that seeks to select the threshold value that maximizes the difference between the averages (inter-class variance) of two classes – background and foreground pixels based on their intensity values – and minimizes the variance within each class (intra-class variance) [74]. All the pixels with values below this threshold are set to 0, while all pixels with values above it are set to 1. Given that the pixels of the stoma are darker than the pixels of the surrounding surface, which is similar to the background in intensity, we should expect the stoma to be easily distinguished with Otsu's method. Consequently, we create a binary mark. From this mask, contours are identified using Suzuki's border-following algorithm [71]. Although this algorithm is designed to not only detect all outlines present in an image but also to organize them into a hierarchy, illustrating their interrelationships or topological structure [71], we solely utilize its ability to detect all outlines. From all the contours extracted from the binary mask by Suzuki's algorithm, we must determine which contour represents the

stoma (Figure 2.12 (b)). To do this, we use the statistical characterization of the contours that typically represent the stoma, following a rules-based approach to keep dataset complexity at a minimum.

For identifying the contour best representing the stoma, we use a scoring system defined by Equation (1). At an overview, the scoring identifies the biggest contour containing the homogeneously darkest set of pixels. The score is inversely related to the mean intensity of the pixels it includes, as a 2.5D image generally depicts the stoma as darker due to its relative height. The score is also directly proportional to the area or number of pixels in the contour for instances where a large contour encompasses a smaller contour that outlines a subset of the stoma. Lastly, the score increases for contours whose pixels have the smallest standard deviation. Offsets are also added to each term where a division by zero is possible. The terms are also further increased by setting large values for exponential variables a and b. From our experiments, we found a and b values of 80 and 3, respectively, worked well.

$$\text{Score} = \text{area} \cdot \frac{1}{(\text{mean pixel intensity} + 0.1)^a} \cdot \frac{1}{(\text{std of pixel intensity} + 0.1)^b} \quad (1)$$

To practically access the pixels within the contour, we obtain a bounding box of a contour. The set of pixels within these bounding boxes from the 2.5D images is used to score the contour. We chose to use the bounding box pixels instead of contour pixels to swiftly determine if a pixel is within the contour, given that many contours might be discovered.

After identifying the highest-scoring contour, the image is cropped to concentrate on the contour with a slight margin on each side (Figure 2.12 (c)), followed by the application of blurring techniques to diminish the clear lines generated by tessellation, thereby encouraging smoother contour extraction. Although we employ Gaussian filtering in our process, we have not tested average filtering firsthand. However, our research suggests that both options seem promising for achieving our goal [75, 76]. It's important to note that filters like median and bilateral, which do not blur lines as efficiently or preserve edges, may not be as effective. In the context of our reconstructed models exhibiting noticeable tessellation in the 2.5D images, we apply multiple blurring filters with small kernels (30x30 and 15x15) to smooth out these effects without causing significant color distortion, which is vital for accurate contour extraction. The identification and scoring process is repeated to ensure accuracy (Figure 2.12 (d)) and extract the final contour (Figure 2.12 (e)).

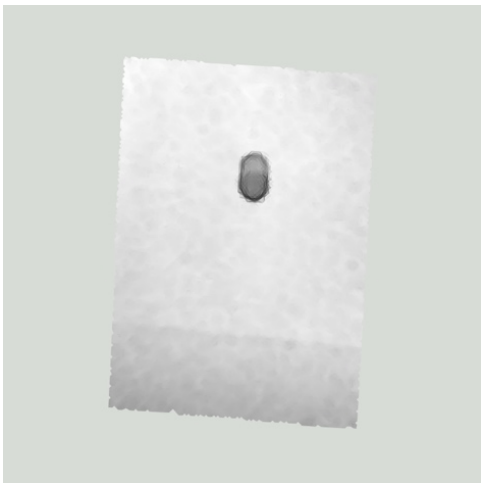

(a)

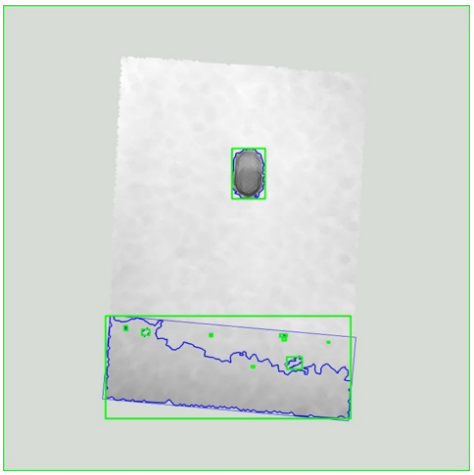

(b)

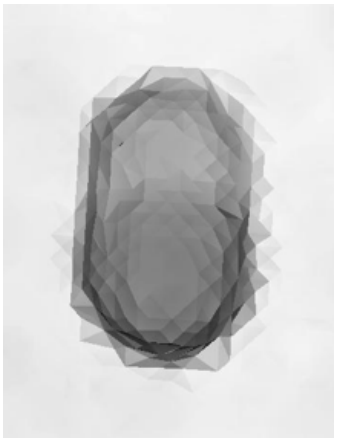

(c)

(d)

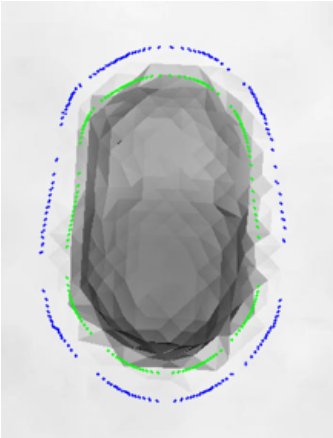

(e)

Figure 2.12: Depicting the contour generation process. Initially, the 3D model is leveled, and a height gradient is applied, producing the overhead snapshot in (a). All potential contours are then identified using OpenCV's algorithm, demonstrated in (b), and each contour is assessed based on Equation (1). The overhead image is subsequently cropped to center the highest-scoring contour, as shown in (c). Within this cropped image, OpenCV's algorithm is used again to discern all contours, shown in (d). The contour scoring highest, which is the central contour around the stoma in (d), is selected. This chosen contour is then expanded by 3.175 mm, as depicted in (e).

2.4.4.4 Error Evaluation

The extracted contours were evaluated with an error-based evaluation: for each pixel in the extracted contour, the minimum Euclidean distance to a pixel on the ground truth contour is computed. To meet our objective, every point on the extracted contour must be less than 2 mm away from a point on the ground truth contour.

2.4.4.5 Contour Expansion

The main objective of this section was to accurately extract the stoma's contour. However, to extend our investigation and demonstrate a proof-of-concept, we also explore contour expansion as the wafer is cut a bit larger than the stoma's contour. According to Nurse Practitioner Quyen Stevenson, for budded stomas, the contour is typically cut 1/8" from the base. If the stoma is mushroom-shaped, the contour is determined from the stoma's widest part. However, for flush or retracted stomas, the contour is cut 1/4" or 6.35 mm from the stoma. Therefore, a machine learning algorithm would ideally be utilized to first identify the stoma type and then apply the appropriate expansion.

For our proof-of-concept of how the stoma's contour could be expanded, we began by calculating the stoma's centroid, which served as our origin. For each point in the contour, we calculated the slope from the centroid (origin) to the point. The goal is to select a point along the line that is the chosen distance away (e.g., 3.175 mm). We used a numerical method for this process. Starting from the centroid and extending past the point on the contour by a distance equal to the distance between the centroid and the point, we placed 100 points along this line. For each of these points, we computed the distance from the centroid. This distance needed to be equal to the original centroid-to-point distance plus 3.175 mm. We iterated through all points until we found one that met or exceeded this distance.

While this method might not yield the exact answer and could potentially introduce some error, any such error should be minimal as the number of points on the line could be increased, resulting in sub-millimeter error. It is worth mentioning that this was merely a proof-of-concept and was not used for any applications beyond illustration, as expanding the contour can be a nuisance process.

Chapter 3. RESULTS

3.1 PRELIMINARY SCANNING RESULTS

This section will delve into the preliminary results derived from scanning a variety of nine objects featuring diverse geometries and textures. These objects were scanned with both a standard reference scanner (NextEngine) and an iPhone 12. Our primary goal was to quantify any potential errors present in the 3D models that the iPhone reconstructed.

3.1.1 *Heatmap Comparison Highlighting Error*

We used CloudCompare to generate annotated heat maps. These heatmaps visually present the distance errors between the models generated by the iPhone and the corresponding ground truth models. A color spectrum ranging from blue to red symbolizes the degree of error; perfect alignment or minimal error is represented by blue, while red is indicative of the relative maximum error. For example, Figure 3.1 serves as an example of the legends within Figure 3.2. Here, an error of 6.66e-4 mm corresponds to blue, while red corresponds to a more considerable error of 3.71 mm. We calculated the absolute distance error for every model, as shown in Figure 3.2, to ensure that we capture the maximum possible error rather than an average, offering a more realistic view of the worst-case scenario.

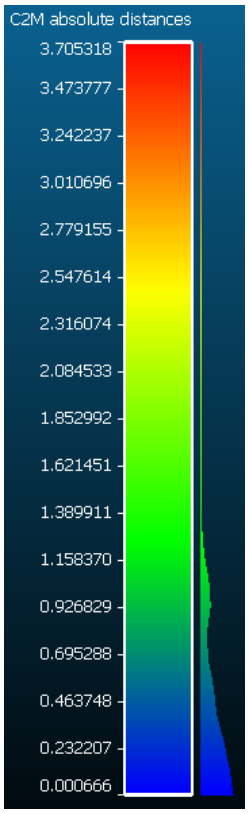

Figure 3.1: The stoma model's heat map legend.

(a)

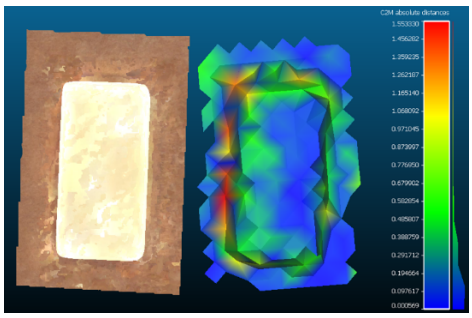

(b)

(c)

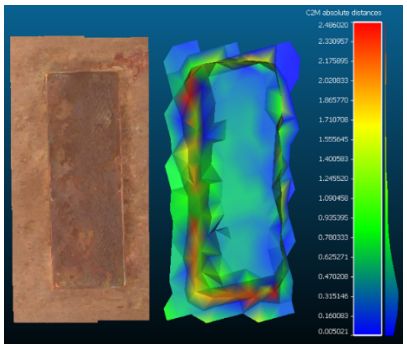
C2M absolute distances

(d)

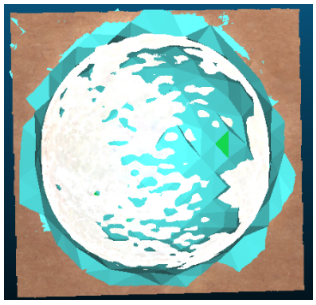

(e)

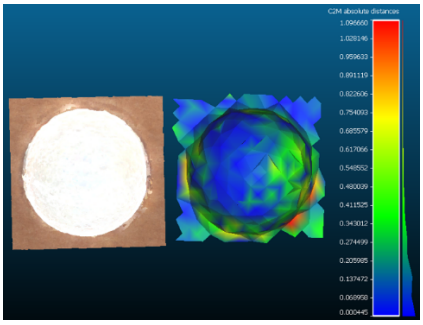
C2M absolute distances

(f)

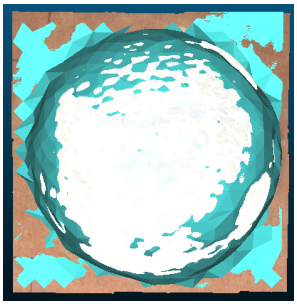

(g)

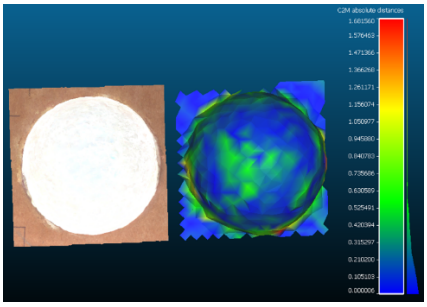
C2M absolute distances

(h)

(i)

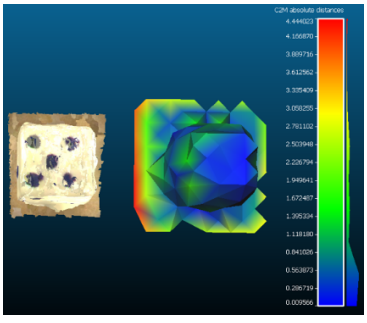
C2M absolute distances

(j)

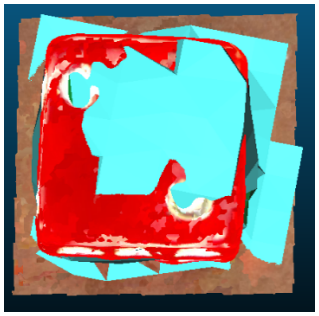

(k)

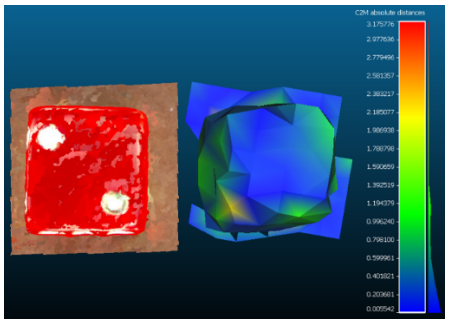
C2M absolute distances

(l)

(m)

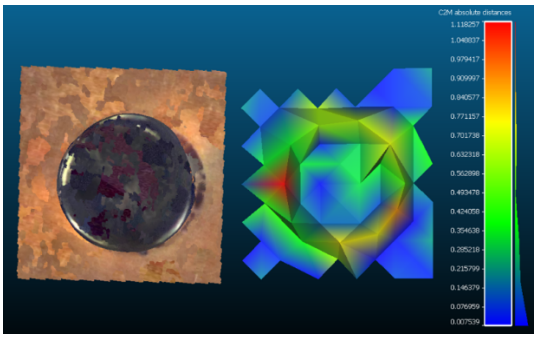
C2M absolute distances

(n)

(o)

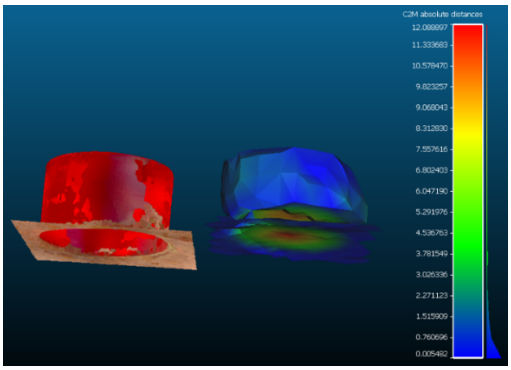
C2M absolute distances

(p)

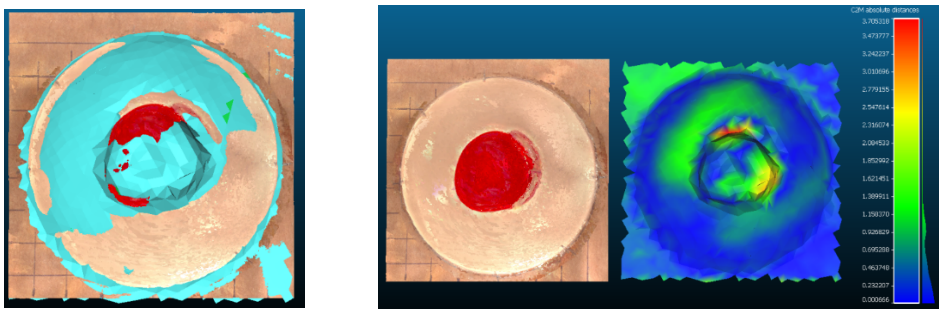

(q) (r)

Figure 3.2: Comparative analysis of model geometry and distance error between iPhone-generated models and NextEngine reference models. The images on the left illustrate the iPhone-generated models (depicted as blue 3D models) merged with the reference models (shown as the colored 3D model): (a) Rectangle 1, (c) Rectangle 2, (e) Half-Sphere 1, (g) Half-Sphere 2, (i) Cube 1, (k) Cube 2, (m) Cylinder 1, (o) Cylinder 2, (q) Stoma model. Correspondingly, the images on the right present the reference model to the left and the iPhone-generated model on the right, which is color-coded according to the distance error from the set of images on the left: (b) Rectangle 1 – error range of 0.001 to 1.553 mm, (d) Rectangle 2 – error range of 0.005 to 2.468 mm, (f) Half-Sphere 1 – error range of 0.001 to 1.097 mm, (h) Half-Sphere 2 – error range of 0 to 1.682 mm, (j) Cube 1 – error range of 0.01 to 4.444 mm, (l) Cube 2 – error range of 0.0056 to 3.176 mm, (n) Cylinder 1 – error range of 0.008 to 1.11 mm, (p) Cylinder 2 – error range of 0.005 to 12.1 mm, (r) Stoma model – error range of 0.001 to 3.705 mm.

3.1.2 *Evaluating Cumulative Distribution of Distance Error*

Recognizing that the scanning process can occasionally yield subpar reconstructions if not carried out carefully, we took three scans for each object using the iPhone to ensure the robustness of our results. We then implemented the procedure to obtain the scalar field of distance error, often referred to as an annotated heatmap, for each model. Saving these models in the PLY-ASCII format allowed us to extract the associated distance error values. We used these values to create the cumulative distribution graphs depicted in Figure 3.3. These graphs effectively demonstrate the percentage of points on the models generated by the iPhone that are within a particular distance (expressed in millimeters) from the reference models generated by the NextEngine scanner.

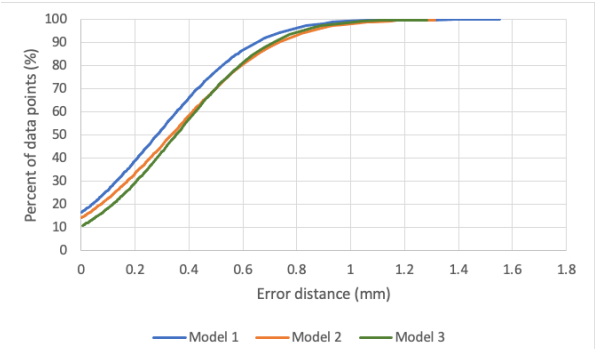
Percent of data points (%)
Error distance (mm)
Model 1
Model 2
Model 3

(a)

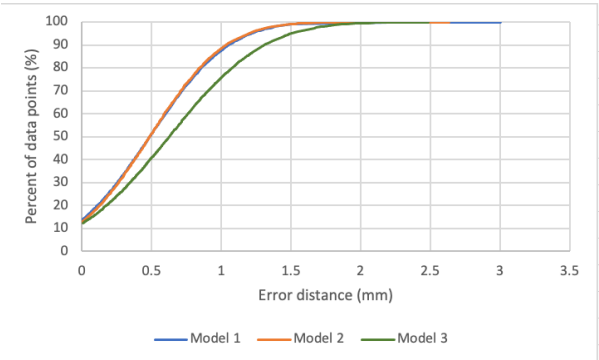
Percent of data points (%)
Error distance (mm)
Model 1
Model 2
Model 3

(b)

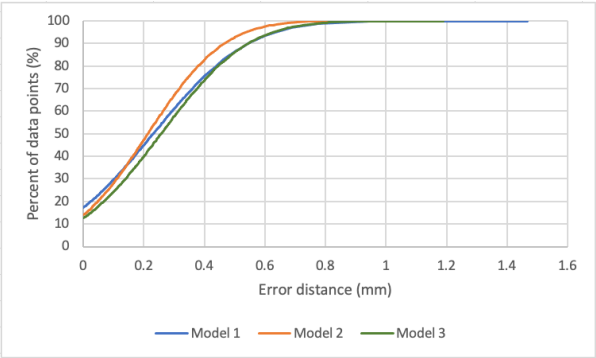
Percent of data points (%)
Error distance (mm)
Model 1
Model 2
Model 3

(c)

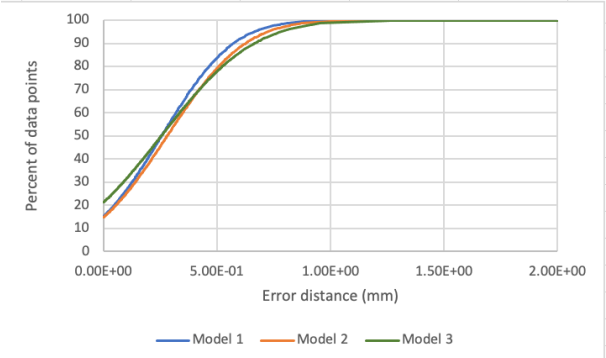
Percent of data points
Error distance (mm)
Model 1
Model 2
Model 3

(d)

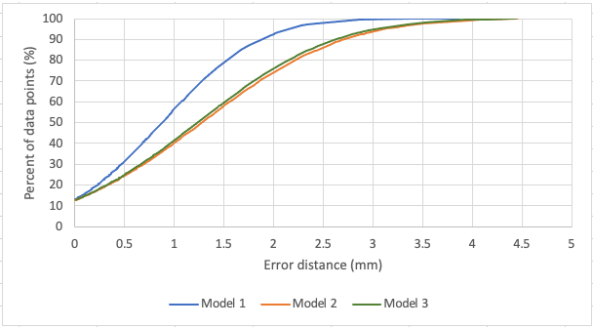
Percent of data points (%)
Error distance (mm)
Model 1
Model 2
Model 3

(e)

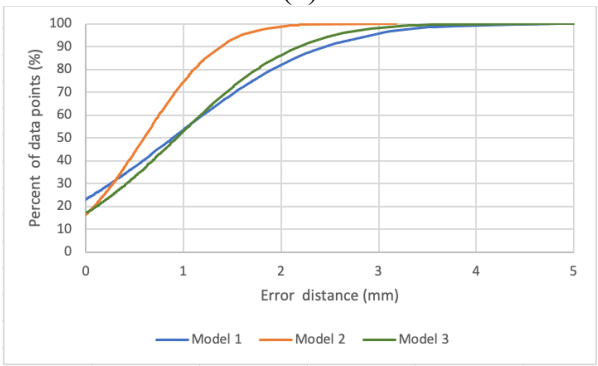
Percent of data points (%)
Error distance (mm)
Model 1
Model 2
Model 3

(f)

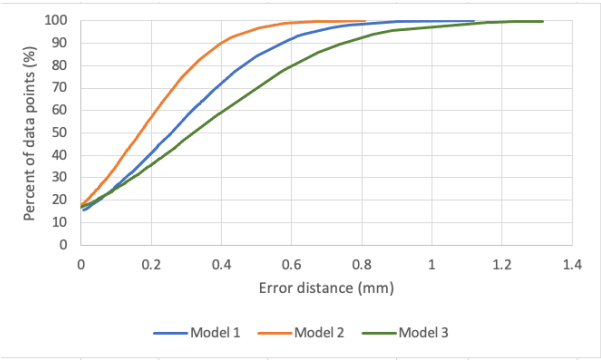
Percent of data points (%)
Error distance (mm)
Model 1
Model 2
Model 3

(g)

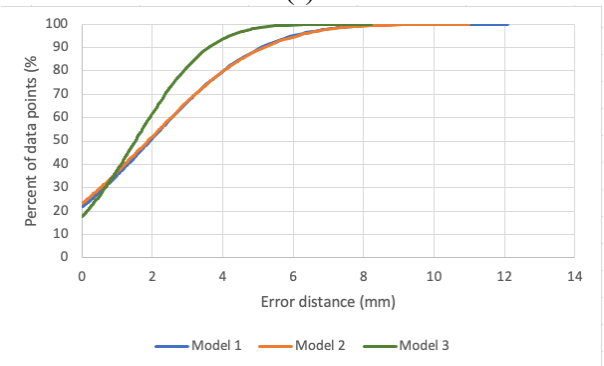
Percent of data points (%
Error distance (mm)
Model 1
Model 2
Model 3

(h)

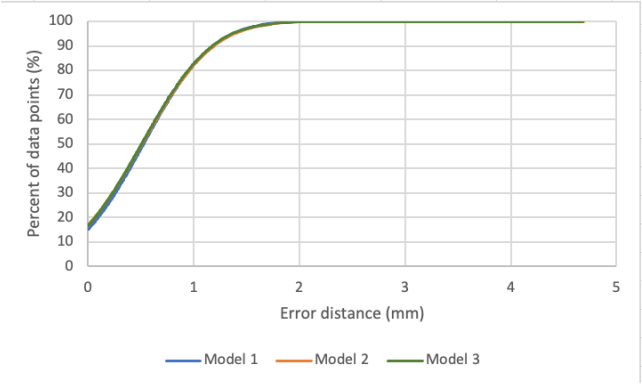

(i)

Figure 3.3: Cumulative distribution plots illustrating the percentage of points on iPhone-generated models that fall within a specified millimeter range from their corresponding reference models. Plots of (a) Rectangle 1, (b) Rectangle 2, (c) Half-Sphere 1, (d) Half-Sphere 2, (e) Cube 1, (f) Cube 2, (g) Cylinder 1, (h) Cylinder 2, (i) Stoma model.

3.1.3 *Assessing Mean Error Distance and Standard Deviation*

Further, we attempted to gauge the accuracy by evaluating the average mean distance error and the standard deviation of three models from the previous section created for each object relative to the ground truth models (Table 5). As mentioned previously, we opted for three models to account for possible variations in the scanning process. It is worth noting that while previous research generally employed a single model or did not specify the number of models used to derive their results [30, 36], they usually obtained various frames or snapshots of an object to compile the frames into a single model comprising as many data points as necessary. Similarly, when using the iPhone application, scanning continues until all the voids are adequately filled; in this process, the software is designed to perform multiple scans and merge them. Nevertheless, various scans should be used to quantify the precision of the results.

Table 5

Average Mean Error and Average Standard Deviation of Scanned Objects

Objects:	Cube 1	Cube 2	Rectangle 1	Rectangle 2
Average Mean Error Distance (mm)	1.1581	0.8034	0.3220	0.5324
Average Standard Deviation	1.0115	0.9298	0.2906	0.4682

Table 5 Continued

Average Mean Error and Average Standard Deviation of Scanned Objects

Objects:	Cylinder 1	Cylinder 2	Half-Sphere 1	Half-Sphere 2	Stoma model
Average Mean Error Distance (mm)	0.2481	1.7728	0.2339	0.2640	0.5135
Average Standard Deviation	0.2498	2.2169	0.2221	0.2788	0.5216

3.2 CONTOUR EXTRACTION RESULTS

We assess the accuracy of our contour extraction algorithm on a sample of fifteen unique stoma models. This analysis yielded diverse results with varying accuracy.

3.2.1 *Contour Overlap*

Table 6 visually compares the ground truth contours and the extracted contours for each stoma model. The first column of Table 6 shows the stoma model images with a green line delineating the ground truth contour, and the second column displays the 2.5D images with the extracted contour also delineated by a green line. The fourth column overlays these contours onto each other; the blue mask corresponds to the ground truth contour, the red mask to the extracted contour, and the purple area highlights the overlap. Note that the X and Y axes represent the distances in millimeters.

Notably, for stoma model S5, the contour extraction algorithm mistakenly selected a section of the 3D model that did not contain the stoma. We also excluded stoma model S10 due to its protruding nature, which impeded us from obtaining the contour at the base of the stoma.

Table 6

Visual Comparison of Ground Truth and Extracted Contours with Overlap

ID	Ground Truth Contour	Extracted Contour	Overlap of Ground Truth and Extracted Contour
S1		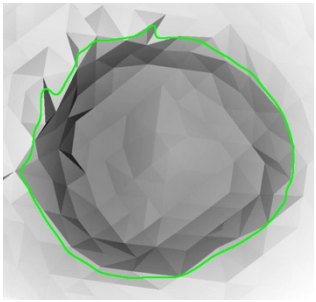	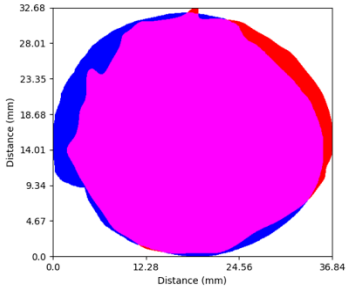
S2		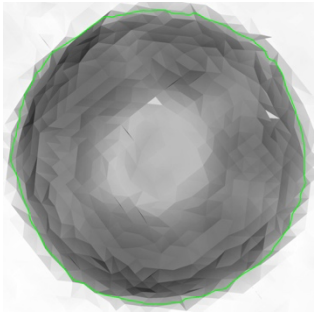	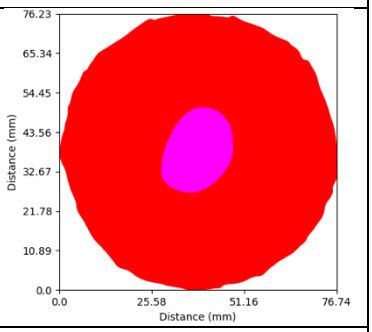
S3		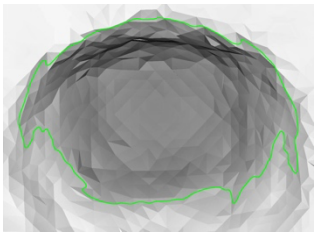	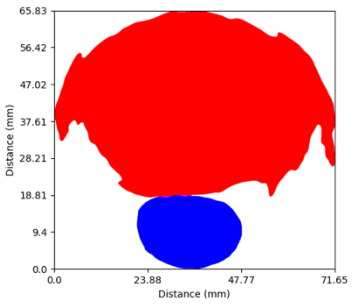
S4		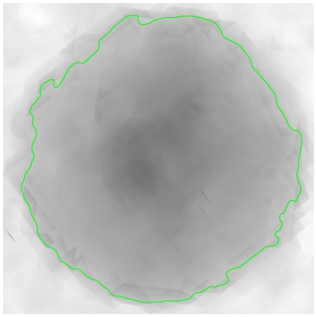	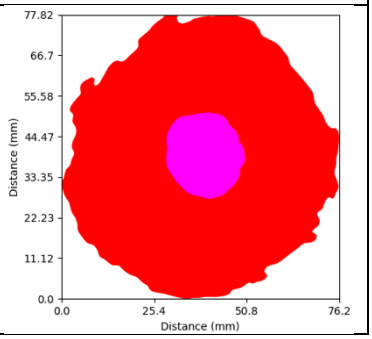

S5			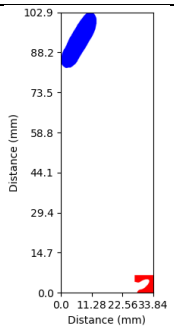 102.9 88.2 73.5 58.8 44.1 29.4 14.7 0.0 Distance (mm) 0.0 11.28 22.56 33.84 Distance (mm)
S6		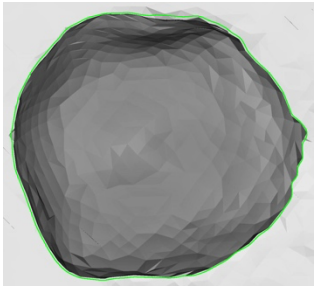	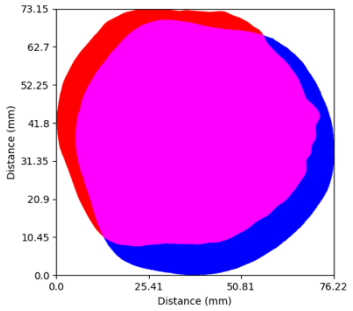 73.15 62.7 52.25 41.8 31.35 20.9 10.45 0.0 Distance (mm) 0.0 25.41 50.81 76.22 Distance (mm)
S7	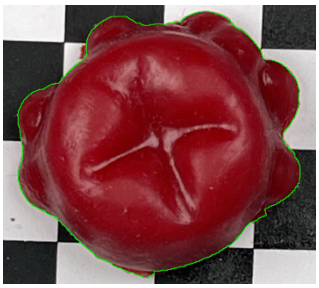	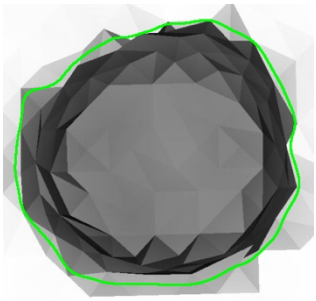	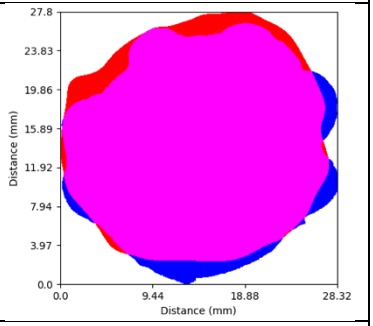 27.8 23.83 19.86 15.89 11.92 7.94 3.97 0.0 Distance (mm) 0.0 9.44 18.88 28.32 Distance (mm)
S8			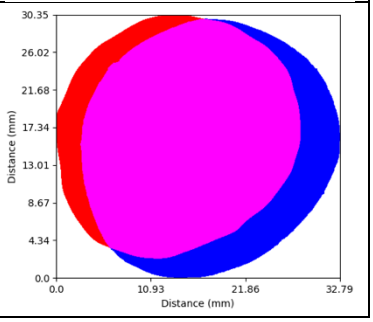 30.35 26.02 21.68 17.34 13.01 8.67 4.34 0.0 Distance (mm) 0.0 10.93 21.86 32.79 Distance (mm)

S9	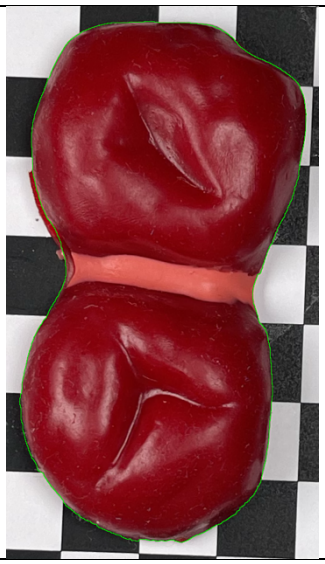	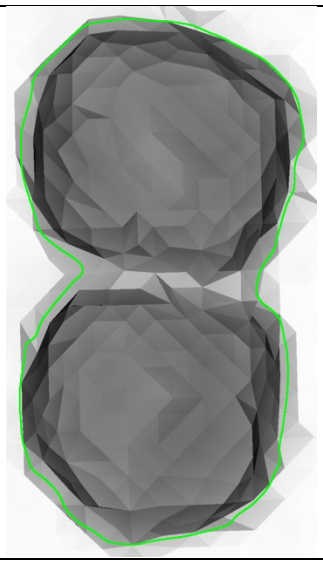	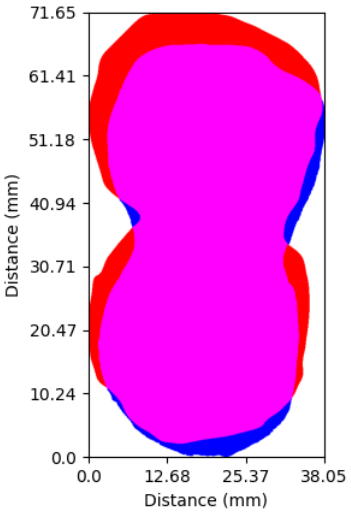
S10	N/A	N/A	N/A
S11		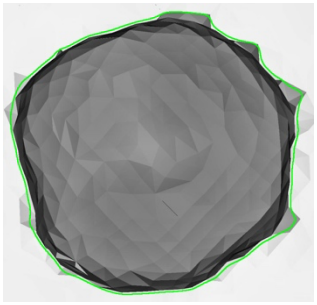	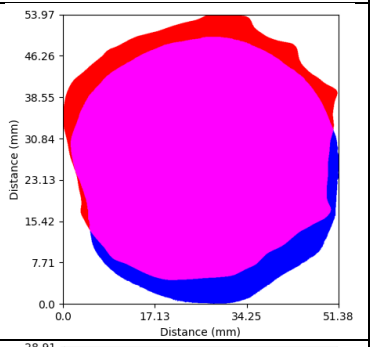
S12		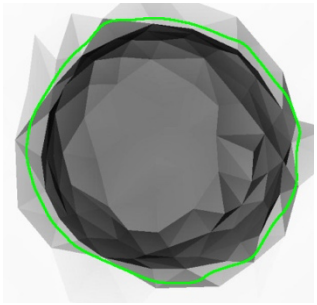	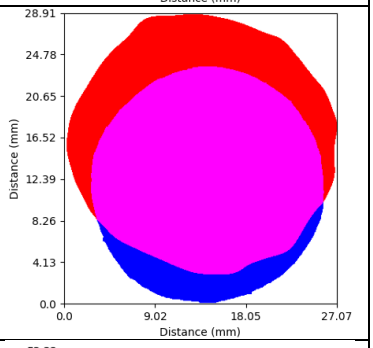
S13		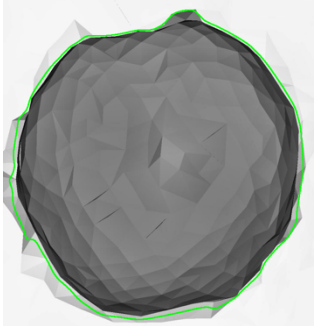	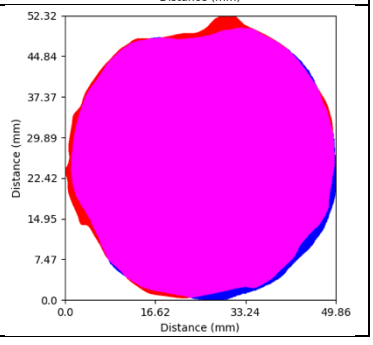

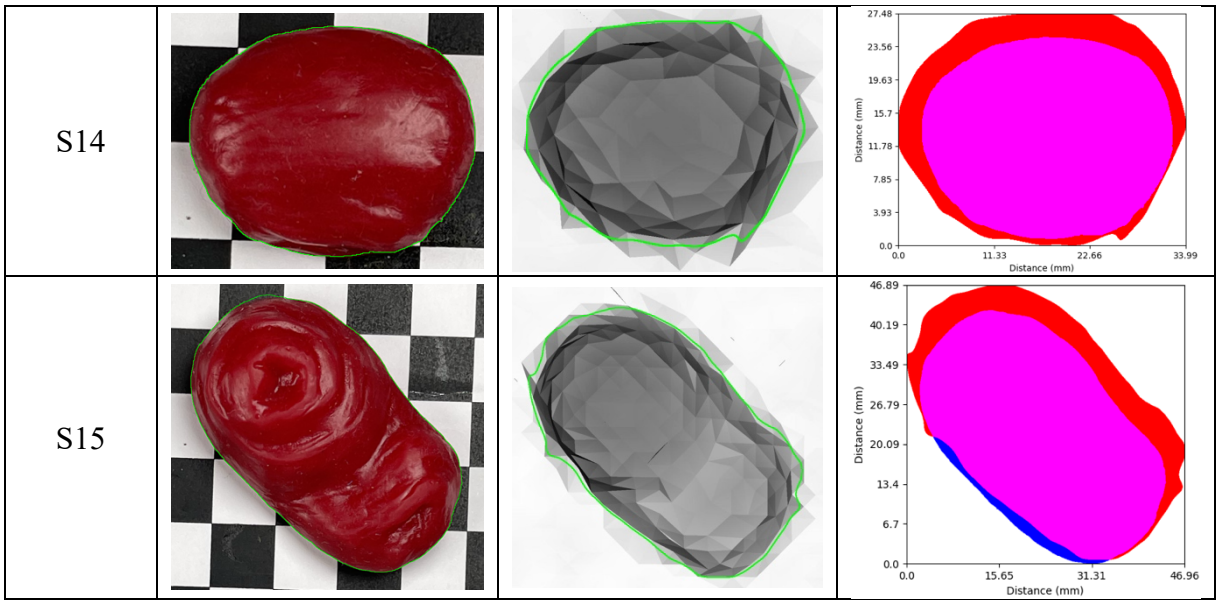

3.2.2 *Error Distribution*

Histograms detailing the distributions of absolute error for each stoma model are shown in Figure 3.4. These histograms show the shortest Euclidean distance to the ground truth contour for every point on the extracted contour. The X-axis illustrates the error distance in millimeters, whereas the Y-axis signifies the frequency of each error magnitude. The error distributions reveal notable differences among the extracted, although most errors are within 6 mm error. Interestingly, the largest errors were found in stomas S2 through S5, a point we will explore in depth in the discussion section.

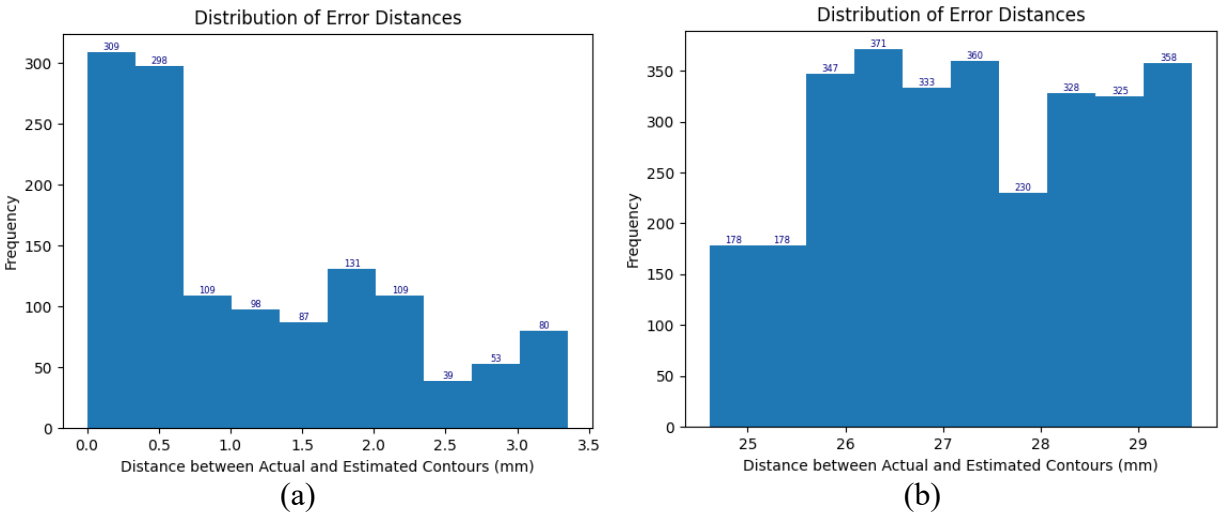

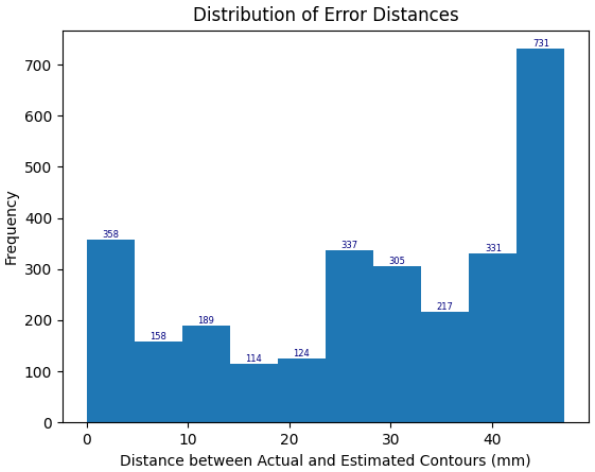
Distribution of Error Distances
Frequency
Distance between Actual and Estimated Contours (mm)
358
158
189
114
124
337
305
217
331
731

(c)

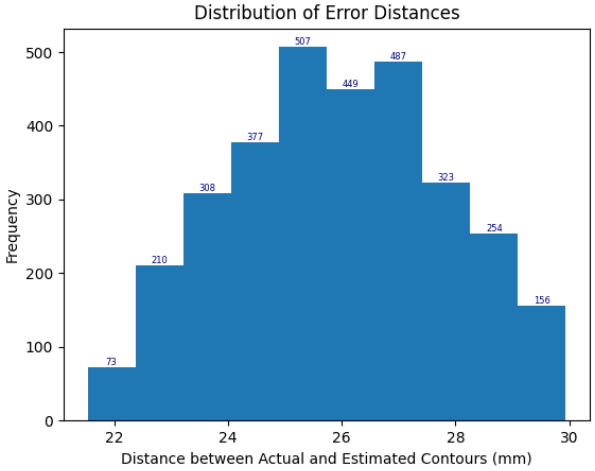
Distribution of Error Distances
Frequency
Distance between Actual and Estimated Contours (mm)
73
210
308
377
507
449
487
323
254
156

(d)

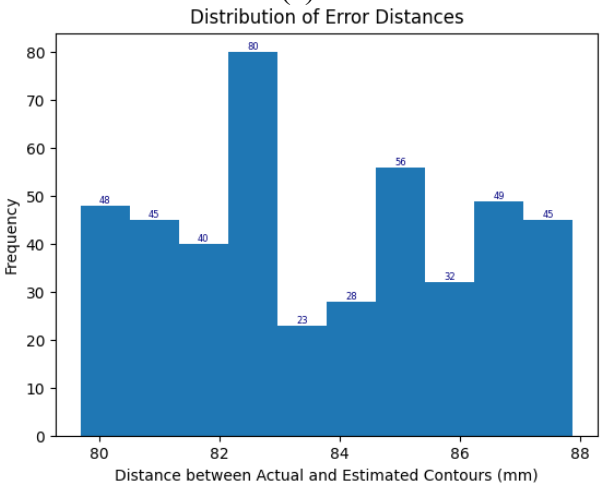
Distribution of Error Distances
Frequency
Distance between Actual and Estimated Contours (mm)
48
45
40
80
23
28
56
32
49
45

(e)

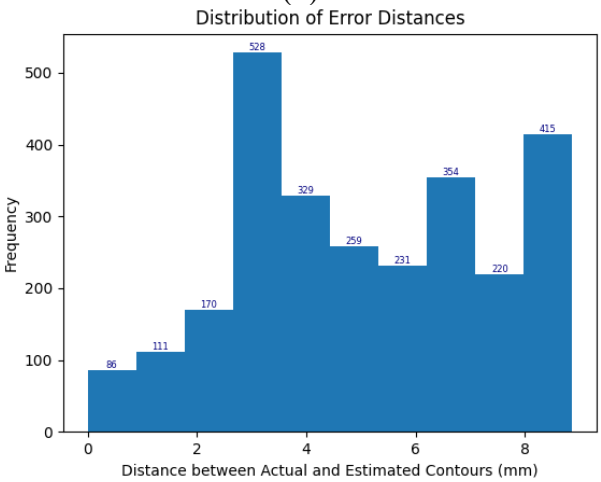
Distribution of Error Distances
Frequency
Distance between Actual and Estimated Contours (mm)
86
111
170
528
329
259
231
354
220
415

(f)

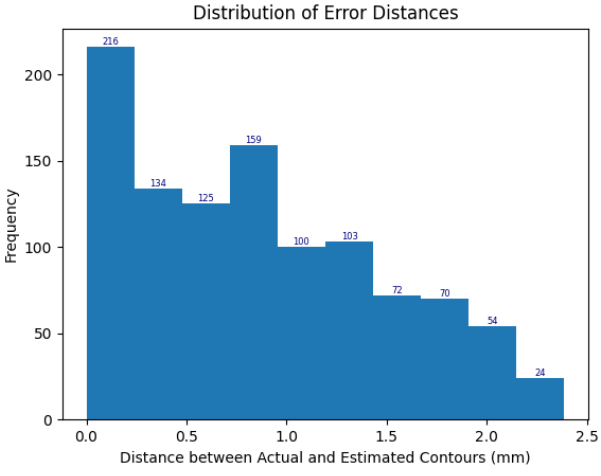
Distribution of Error Distances
Frequency
Distance between Actual and Estimated Contours (mm)
216
134
125
159
100
103
72
70
54
24

(g)

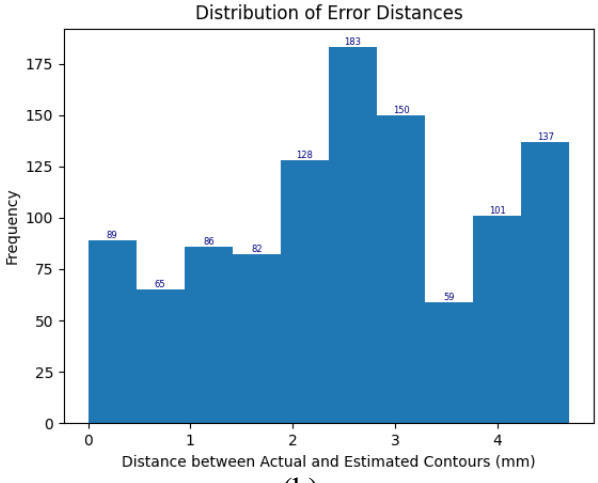
Distribution of Error Distances
Frequency
Distance between Actual and Estimated Contours (mm)
89
65
86
82
128
183
150
59
101
137

(h)

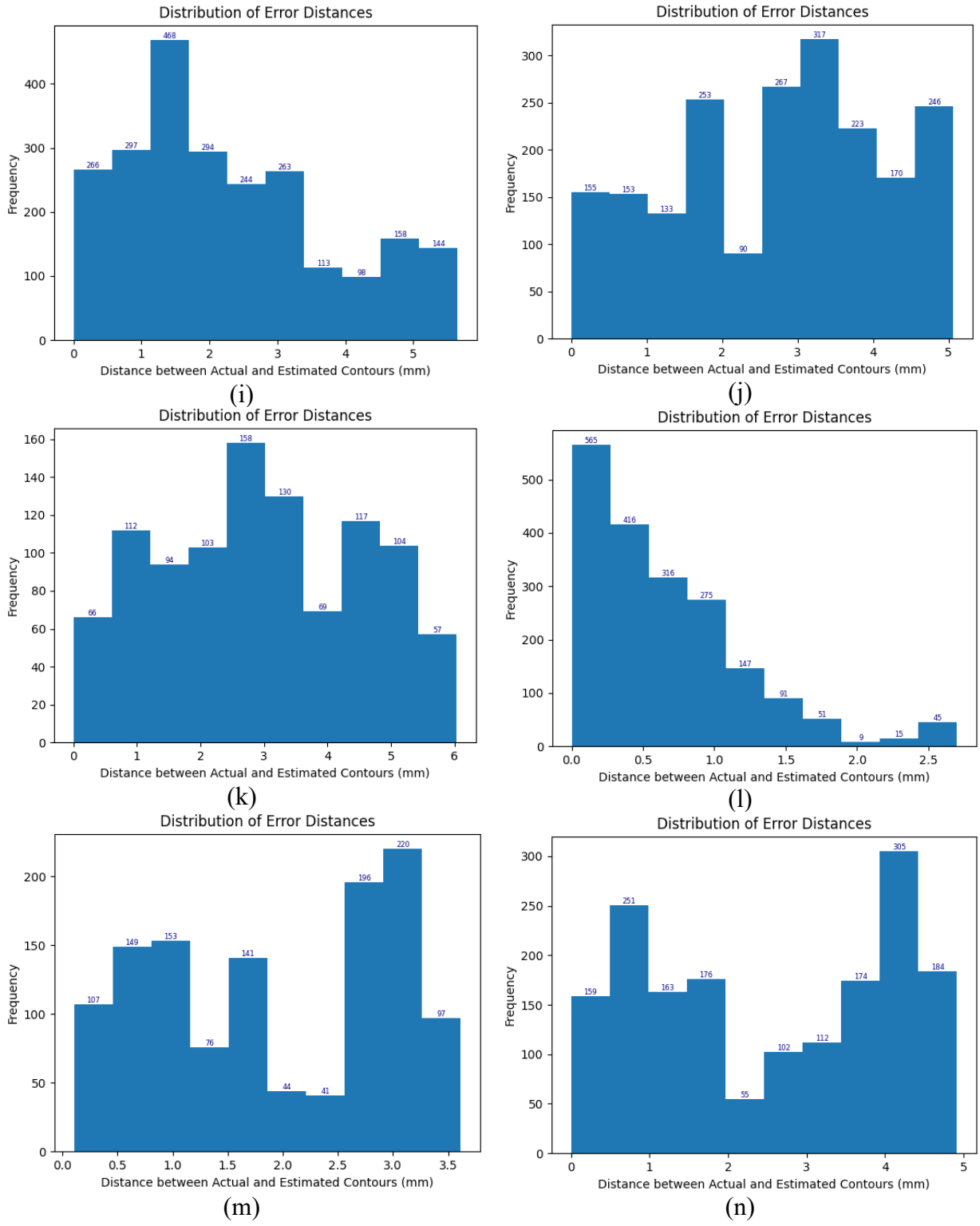

Figure 3.4: Histograms depicting the error distances between ground truth and extracted stoma contours. Each histogram represents the frequency (y-axis) of error distances (x-axis) of each

stoma model: S1 (a), S2 (b), S3 (c), S4 (d), S5 (e), S6 (f), S7 (g), S8 (h), S9 (i), S11 (j), S12 (k), S13 (l), S14 (m), S15 (n).

3.2.3 *Statistical Analysis of Error*

Table 7 provides further statistical insights into the discrepancies between the extracted and the ground truth contours. It includes each stoma model's minimum, maximum, average error, and standard deviation. These details provide a more granular understanding of the range and distribution of the errors.

Table 7

Detailed Statistical Analysis of Distance Errors for Each Stoma Model

Stoma Model	**Minimum Error (mm)**	**Maximum Error (mm)**	**Average Error (mm)**	**Standard Deviation (mm)**
S1	0.0	3.36	1.16	0.95
S2	24.61	29.56	27.26	1.35
S3	0.0	47.17	28.12	15.46
S4	21.53	29.94	25.94	1.93
S5	79.68	87.88	83.69	2.43
S6	0.0	8.87	5.03	2.29
S7	0.0	2.39	0.87	0.62
S8	0.0	4.71	2.52	1.28
S9	0.0	5.65	2.3	1.5
S11	0.0	5.07	2.76	1.4
S12	0.0	6.04	2.98	1.58
S13	0.0	2.7	0.67	0.55
S14	0.1	3.62	1.92	1.06
S15	0.0	4.92	2.54	1.54

Chapter 4. DISCUSSION

The primary objective of this research was to create the system depicted in Figure 1.3 to aid ostomy patients in procuring custom-fit ostomy wafers. As outlined in the methodology section, two research-intensive aspects of this system required development. The first entails the validation of the iPhone, which we deemed the most suitable scanning device, to reconstruct objects accurately. Our preliminary scanning experiments confirmed this, where six out of nine objects demonstrated nearly 100% of points on the reconstructed models falling within 2 mm of the reference models. The process, however, unveiled that scanning objects requiring circular, side-angle movements led to more distorted models.

The second developmental component involved developing algorithms that generate the optimal stoma contour given a 3D model of the stoma. We used fifteen stoma models to test the algorithm, which incorporates Suzuki's contouring algorithm. This experiment revealed that nine of the fifteen extracted contours had a maximum error of 6 mm. Although errors did occur in the scanning and contour generation process, these inaccuracies do not negate the iPhone's potential for application in this context, as there are clear areas for improvement. We will delve deeper into the results in the following sections.

4.1 Discussion on Preliminary Scanning Results

The objects scanned—rectangle 1, rectangle 2, cylinder 1, half-sphere 1, half-sphere 2, and the stoma model—exhibited the highest accuracy, with 75% of points (third quartile) falling approximately 1 mm from the reference models, as demonstrated by the annotated heatmaps. Nevertheless, tessellation became apparent where the objects met the background surface or in objects with abrupt edges like rectangle 1, rectangle 2, and cylinder 1, leading to distorted models. This distortion became even more pronounced with cube 1, cube 2, and cylinder 2, suggesting that objects with surfaces containing gradients much less than 90 degrees are best represented.

Moreover, the images do not reflect the difficulty in capturing certain objects, such as rectangle 2 and cylinder 2. Multiple scanning attempts were required for these objects because they necessitated side perspective scans, during which the application may create distorted models. The infinitam_ios application occasionally lost track during this process and had to be restarted. Moreover, improper scanning of the object's sides resulted in incomplete scans, as shown in Figure 4.1, where the upper half of the cylinder is visibly cut off from the background surface.

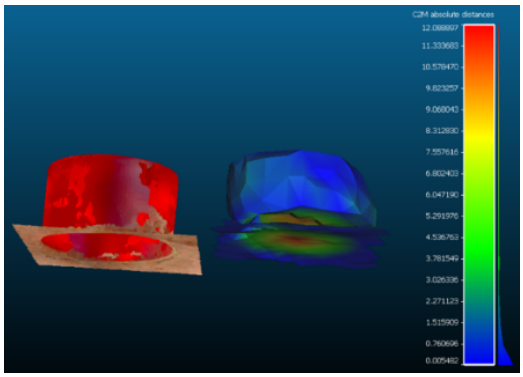

Figure 4.1: A comparison of the side-perspective view of the reference model (left) and the iPhone-reconstructed model (right) for Cylinder 2. The image highlights the distortion in the iPhone-reconstructed model, with the upper half appearing to be cut off from the background surface, demonstrating one of the challenges encountered in the 3D scanning process.

In the case of the stoma model, the primary source of error appears to stem from potential misalignment with the reference model. Due to tessellation, the mucocutaneous separation, depicted as a dip to the right of the red stoma spout, might be aligned above the stoma in the iPhone-reconstructed model.

These results indicate that objects entirely capturable from an overhead perspective are captured with an accuracy exceeding 2 mm, surpassing the results in [30] and marginally bettering the results for the Structure Sensor in [36]. However, improvements to the scanning application are necessary to enhance accuracy and facilitate the scanning of tall and protruding stoma spouts, especially those obstructing peristomal skin from an overhead perspective.

4.2 Discussion on Contour Generation Results

Our experiment used fifteen stomas, with one (S10) being excluded due to the stoma's protruding nature obscuring the base, preventing us from extracting both the ground truth and test contour. Five stoma models had stomas surrounded by skin, each presenting unique surface geometries. For instance, S1 represented a typical stoma spout with a slight separation from the surrounding skin. S2 was a recessed stoma, such that the surrounding skin was taller; S3 was nearly leveled with the skin and was placed by a hernia; S4 was a flush stoma, so the tip of the stoma was leveled with surrounding skin, and S5 was situated within a body crease. The diverse peristomal and stoma geometries in S2 through S5 made it difficult for the algorithm to identify the stomas using their topology, thus resulting in average errors exceeding 25 mm for these models.

The remaining stomas, although identified correctly, demonstrated varying degrees of accuracy. However, all maintained an average error of less than 3 mm, with the maximum error of 8.87 mm observed in S6. Some errors can be attributed to misalignment between the ground truth

and extracted contours, as shown in S6, S8, S9, S11, S12, and S15, and minor inaccuracies might be due to tessellation introduced by the infinitam_ios application, as shown in S1.

As an initial approach, we developed a rules-based contour algorithm using 2.5D images to minimize the complexity of establishing a 3D workflow. This was feasible as the stoma's optimal contour can be extracted from an overhead perspective. While the achieved accuracy did not meet our target, the maximum 8 mm error for nine of the fifteen models suggests greater potential in integrating 3D components into the process. This strategy bypasses common errors associated with 2D imaging, such as illuminance and capture angle variations, while being relatively simple. Scanning the models was similar to recording a video, making this system practical for ostomy patients to use from home.

However, our findings underscore the necessity of a 3D workflow to handle the complexities of stomas effectively; further explanation will be provided in the limitations section. We suggest adopting a learning-based approach for robust-stable results. Additionally, improving the 3D scanning and reconstruction processes to reduce tessellation and incorporate color into the final model could contribute to more accurate outcomes. These enhancements would facilitate alignment between the model and the ground truth image, promoting accuracy.

4.3 Real-World Implementation Considerations

Considering that the average ostomy patient is around 70 years old [77], it is reasonable to question whether these individuals would be comfortable using or even have access to a smartphone to utilize this system. The study conducted in [55] provides encouraging evidence, demonstrating that elderly patients (mean age: 70 years, range: 41 to 87 years) were willing and able to use a smartphone for wound care surveys. This finding holds relevance to our system, suggesting potential usability among the elderly demographic. Further supporting this, our application boasts large, easily navigable buttons and an intuitive user interface. The scanning process resembles video recording, a task many smartphone users are familiar with. To ensure maximum usability, we would also develop tutorial videos to assist patients who may struggle initially.

An area that warrants further exploration is the impact of patient positioning during the scanning process. The generated contour could differ depending on whether the patient is standing or lying down. Additional studies are required to establish the optimal positioning that results in an extracted contour that most closely resembles the contour a nurse would use in ostomy patient care.

Similarly, the contour generation process requires further refinement. While our research was able to extract somewhat precise contours of the stoma and demonstrated a potential method for expanding this contour, our approach may not always be the most suitable. For instance, if jagged edges are produced during exact contour extraction, and these are expanded, a nurse may prefer a smooth, rounded contour for the patient's comfort and safety. Furthermore, considering the possible implications of an incorrectly customized wafer, we must establish robust procedures to handle errors or inaccuracies. This could involve a nurse reviewing and verifying each extracted

contour or enabling patients to confirm and make adjustments to the algorithmically extracted contour.

Lastly, the process of customizing the wafers demands consideration. Given the unknown and potentially hazardous materials in each wafer, laser cutting may not be safe. Alternative methods, such as CNC milling or physical etching, should be investigated for wafer customization. As demonstrated in Figure 4.2 and Figure 4.3, an ostomy wafer can be taped to a milling bed, with the resulting customized wafer fitting comfortably onto the stoma. An important feature of the wafers produced by this process is their smooth edges. Nurse Practitioner Quyen highlighted a significant benefit of this system—its capability to produce wafers with smooth edges, thus preventing unnecessary trauma and damage to the stoma, which might overwise occur when patients adjust their wafers. As the wafer is worn all day, continual friction against the nerveless intestinal spout can pose a risk. Therefore, a smooth edge wafer can help prevent unnecessary harm to the intestine.

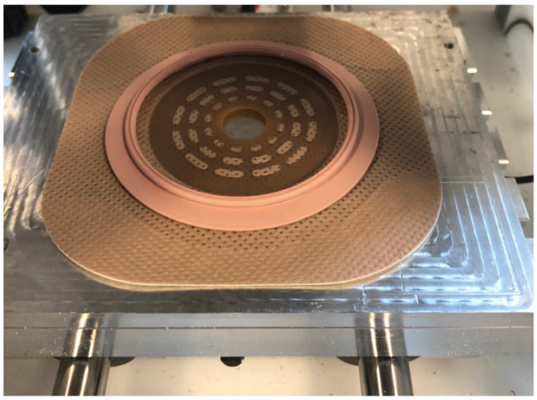

Figure 4.2: An ostomy wafer taped to a CNC milling bed.

Figure 4.3: A ostomy wafer customized with a CNC mill placed onto an ostomy model.

4.4 Other Implementation Considerations

Several other considerations must be taken into account for implementing this system, ranging from legal aspects to business feasibility.

Firstly, a question often asked is whether the customization process needs to sterilize the ostomy wafer. Sterilization is unnecessary since the wafer will not be applied to a sterile environment. Nurse Practitioner Quyen substantiated this insight, noting that patients frequently cut their ostomy wafers up to several weeks ahead of time once the ostomy site stabilizes, leaving the wafers exposed.

Secondly, from a technical standpoint, our research indicates that only iPhones equipped with the TrueDepth system are compatible with our proposed solution due to the system's capacity to capture accurate depth measurements. Other phones may have depth-sensing capabilities, but these capabilities are limited to one or two phones in each brand, making the effort value tradeoff questionable.

From a business perspective, the system's viability remains questionable. Through over 150 interviews with ostomy patients, WOC nurses, surgeons, and professionals in ostomy care, we have found that only a minor proportion of patients struggle with wafer customization. Several WOC nurses indicated that out of the hundreds, if not thousands, of ostomy patients they have assisted, fewer than ten patients each required customized wafers. Furthermore, patients we interviewed perceived wafer customization as a tolerable inconvenience rather than a severe problem, rendering our service more of a luxury than a necessity. The prevalent solution to avoid the wafer inflicting harm on the intestinal spout is to cut the wafer larger than the spout and use eakin rings, which mold to the stoma shape and protect the skin from bodily waste. Industry insiders also note that ostomy supply distributors are unlikely to invest in additional technology due to the narrow profit margins in ostomy care. Currently, within the industry, Byram Healthcare offers a rough customization program, as shown in Figure 4.4, and brief interviews with managers at Byram suggest this program is sufficient as-is. However, the capacity to scan objects and extract their state information could offer benefits beyond wafer customization, potentially facilitating ostomy site monitoring in a telehealth or home health setting.

We would likely need FDA approval to use this system for ostomy wafer customization or monitoring. We could initiate the FDA regulatory process with a pre-submission meeting to confirm if the 510k premarket notification process suits our medical device/software.

Moreover, if we were to provide ostomy measurements to healthcare providers, the system would need to integrate with existing healthcare electronic medical records. This would necessitate careful consideration of the system's compatibility with existing healthcare processes and systems, particularly concerning data exchange and privacy.

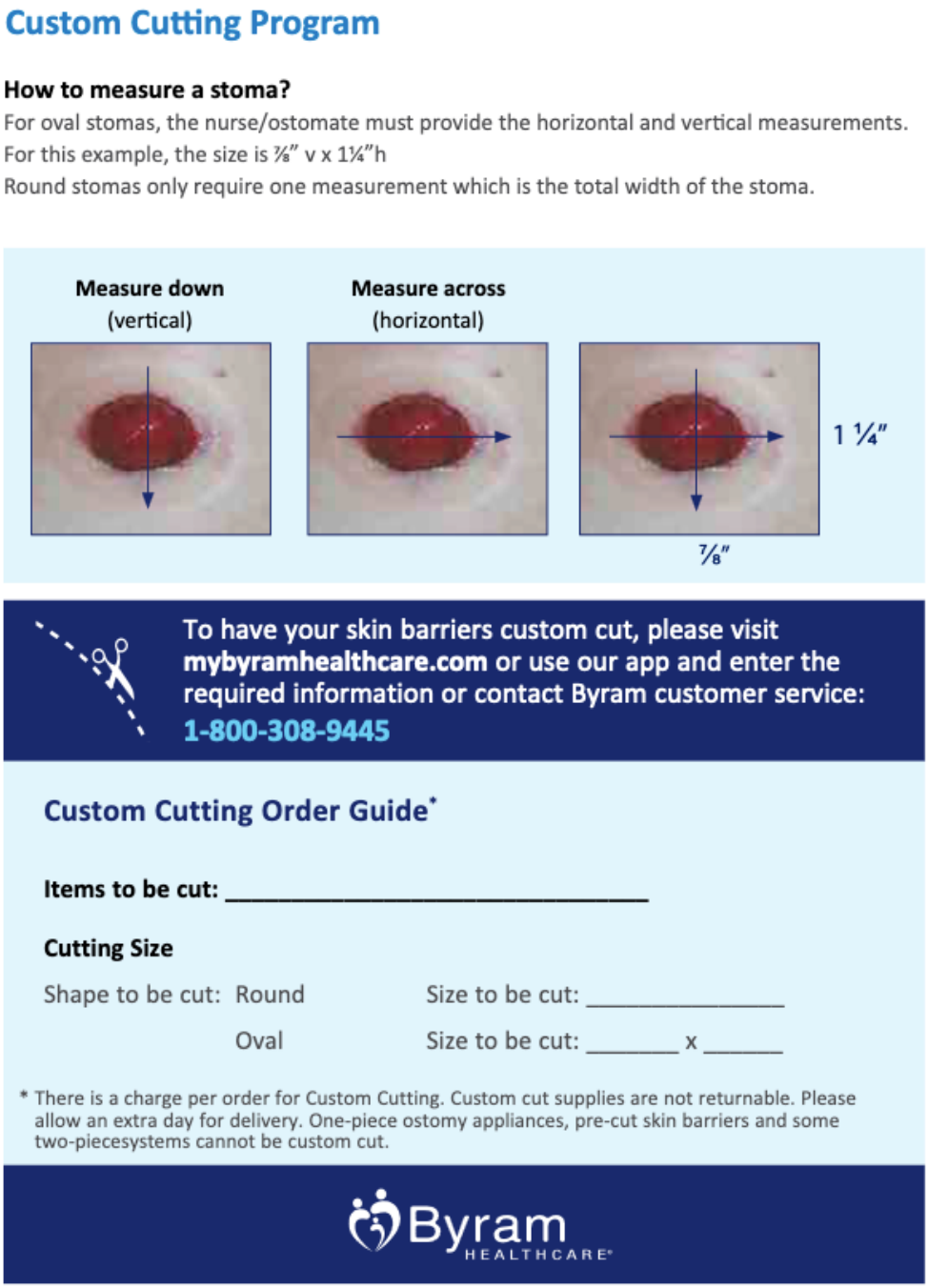

Figure 4.4: Byram Healthcare's customization program roughly customizes ostomy wafers with major and minor axis measurements of the ostomy [78].

Chapter 5. LIMITATIONS AND FUTURE WORK

Although the results of our research into the development of the system depicted in Figure 1.3 did not entirely meet our initial objectives due to inaccuracies in the scanning process and complexities surrounding accurate stoma contour, this work has undeniably taken a critical stride towards supporting ostomy patients in their stoma management endeavors. This chapter aims to delve into the limitations we encountered during our research, the implications these shortcomings had on our findings, and the necessary strides that future work should take to overcome these challenges and maximize the potential of our proposed system.

5.1 LIMITATIONS OF PRELIMINARY SCANNING EXPERIMENTS

As discussed in the previous chapter, one significant technical challenge encountered was scanning objects with a height exceeding 15 mm, requiring the capture of side surfaces. Quick or sudden movements often resulted in the scanning application losing track of the object, necessitating a restart of the application. We believe this is due to the application's real-time snapshot stitching approach, which attempts to merge current depth samples with the ongoing 3D model generation. Objects such as half-spheres needed to be scanned swiftly due to their symmetrical nature, which made it easy for the application to lose track during the merging process. We envision that utilizing other iPhone sensors could potentially aid the reconstruction process, thereby improving the accuracy of frame merging.

As for the final 3D scans, they provided a reasonable starting point, but future improvements should focus on enhancing accuracy and incorporating color. The cause of tessellation will need further investigation to determine whether it signifies a limitation of the TrueDepth sensor's resolution or an issue stemming from the registration/reconstruction process that can be addressed. During our experiments, we attempted to use a tile of known dimensions to scale the iPhone models in CloudCompare appropriately. Unfortunately, the tile's edges lacked clear definition, providing no definitive reference points (Figure 5.1). Utilizing the outer blue polyline as a reference resulted in under-scaled models while referencing the inner pink polyline led to a minor over-scaling.

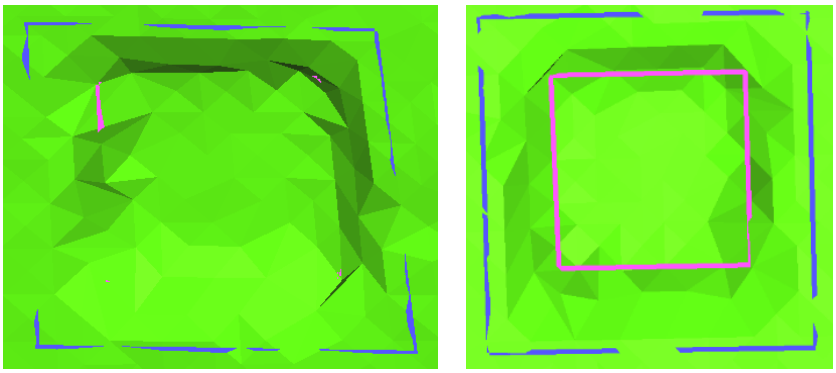

(a) (b)

Figure 5.1: Reference tile with polyline tracing indicating possible marks to use. (a) Overhead scan. (b) Underside scan.

In our work, we evaluated the capability of the iPhone 12's TrueDepth system to replicate eight objects of similar size to a stoma, as well as a stoma model itself. When comparing the iPhone-generated models with those produced by the NextEngine scanner, we found that the iPhone 12 could accurately replicate objects that were captured mainly from an overhead perspective. Nonetheless, the accuracy leaves room for improvement, and the application must be enhanced to facilitate scanning objects that require more varied moments. The difficulties with scanning were particularly evident with Cylinder 2, for which we could not obtain scans that adequately captured the sides, resulting in the largest error among all models. It is conceivable that taller objects would present even greater challenges for accurate capture.

Moving forward, our work will aim to improve model accuracy by refining the scanning application. However, before we proceed, we acknowledge the necessity of characterizing the TrueDepth sensor with a similar methodology as undertaken in [36, 38, 39] to explore other 3D sensors. This will allow us to understand the sensor's inherent limitations better and determine whether enhancements to the registration algorithm would be sufficient to make the application suitable for use in this context. As part of this process, we will need to ascertain where improvements to the scanning protocol can be achieved using the existing Infinitam framework [69] or whether we should develop our algorithm. Ideally, the revised process should utilize additional phone sensor information to overcome issues with tall and symmetrical objects and generate colored 3D models with minimal tessellation.

5.2 Limitations of Contour Generation

This study explores using the iPhone 12 to reconstruct stoma models, from which we generated 2.5D images to explore a methodology for precise stoma contour extraction. Out of the fifteen stoma models utilized, one had to be excluded due to the inability to extract the contour. Of the remaining fourteen, nine demonstrated a maximum error of 6 mm, one exhibited a maximum error

near 9 mm, while the rest incorrectly identified the stoma, leading to substantial errors. Apart from the misidentification of stomas, the primary sources of error were linked to proper alignment and tessellation in the 3D models.

A fundamental limitation of our study was that stomas were placed on a flat surface. However, as observed with stoma models S2 through S5, this method fails to accurately account for the complex topographical conditions of actual stomas. Furthermore, real-life stomas, which could be in more intricate situations like a prolapsed stoma (S10), cannot be accurately scanned with the current application, as we observed in the previous section.

Additionally, the scanning application's inaccuracies and lack of color representation hindered our ability to identify clear reference points for aligning the ground truth and 2.5D images. The manual alignment necessary due to this may have further contributed to the misalignment error.

Looking forward, future studies should consider including stomas situated on mannequins to expand the scope of research. Further improvements should focus on enhancing the 3D scanning process, incorporating color into the 3D models, and employing learning-based algorithms for processing 3D models. Such advancements will provide a more detailed and accurate representation of stomas, subsequently improving the precision of contouring. Our study lays the groundwork for further explorations in this field, and these advancements can help to enhance stoma care and management.

Chapter 6. CONCLUSION

Presently, millions of ostomy patients rely on dated equipment for adjusting their ostomy wafers, an essential component for safeguarding the surrounding skin from bodily waste exuding from their surgically creating stoma. Ill-fitting wafers can potentially lead to severe complications, ranging from unnoticed bleeding caused by tightly fitting wafers to skin erosion and infection due to loosely fitting wafers. To mitigate these problems, we initiated the development of the Osto-Mate system. This low-cost, user-friendly solution leverages the depth-sending capabilities of smartphones to capture a detailed, three-dimensional profile of the stoma and generate an optimal contour for customizing wafers.

The Osto-Mate system, primarily designed with elderly ostomy patients in mind, offers an intuitive application that allows easy stoma scanning. The scan data is then transferred to a database and processed on a server using a contour extraction algorithm. The generated contour is expanded and re-uploaded. Given the potential self-adjustment errors patients can introduce, we explore commercializing the system to deliver customized wafers; however, such a system brings up some challenges.

By probing into the possibilities and constraints of readily available devices, we have pioneered a method to extend advanced services to patients with limited options, promoting better healthcare equity. For future endeavors, it would be valuable to consider research on stomas placed on mannequins to broaden the scope. Enhancements to the current system entail refining the 3D scanning process, integrating color in the 3D models, and applying learning-based algorithms to process these models. This would offer a more precise and detailed representation of stomas, improving contouring accuracy.

Despite our discovery that the problem we initially set out to solve may not be as widespread as we initially thought, our work still paves the way for novel explorations in stoma care. We remain optimistic that such advancements can significantly improve stoma management. Therefore, our work is a stepping stone for future research aiming to enhance the lives of ostomy patients in a similar manner.

REFERENCES

[1] F. L. Monroy, R. Hussein, and A. Mamishev, "Accuracy of Smartphone Depth Cameras in Stoma Shape Extraction for Wafer Fitting," in *2022 Signal Processing: Algorithms, Architectures, Arrangements, and Applications (SPA)*, 2022: IEEE, pp. 40-45.

[2] F. Luquin Monroy and R. Hussein, "Contour Extraction of Surgical Stoma Surfaces Using 2.5D Images from Smartphone 3D Scanning," presented at the Signal Processing: Algorithms, Architectures, Arrangements, and Applications, 2023.

[3] *New Ostomy Patient Guide*: United Ostomy Associations of America, Inc. The Phoenix, 2021. [Online]. Available: https://www.ostomy.org/wp-content/uploads/2020/10/UOAA-New-Ostomy-Patient-Guide-2020-10.pdf.

[4] United Ostomy Associations of America, American Association for Homecare, United Spinal Association, Wound Ostomy and Continence Nurses Society, and Wound, Ostomy, and Continence Nursing Certification Board, *The Critical Need to Provide Ostomy Supplies Specific to Patient Need to Improve Health Outcomes*. 2021. [Online]. Available: https://www.wocn.org/wp-content/uploads/2021/08/9a_AAH-Ostomy-White-Paper-FINAL-07-08-21.pdf.

[5] L. R. Miller and B. M. Peck, "Patient-centered care: an examination of provider–patient communication over time," *Health Services Research and Managerial Epidemiology,* vol. 6, 2019.

[6] H.-W. Seo, "Effects of the frequency of ostomy management reinforcement education on self-care knowledge, self-efficacy, and ability of stoma appliance change among Korean hospitalised ostomates," (in eng), *International wound journal,* vol. 16 Suppl 1, no. Suppl 1, pp. 21-28, 2019.

[7] M. Khalilzadeh Ganjalikhani, B. Tirgari, O. Roudi Rashtabadi, and A. Shahesmaeili, "Studying the effect of structured ostomy care training on quality of life and anxiety of patients with permanent ostomy," (in eng), *International wound journal,* vol. 16, no. 6, pp. 1383-1390, 2019.

[8] Y. S. Feitosa *et al.*, "Causes attributed to stoma or peristomal skin complications in northeast Brazil," *World Council of Enterostomal Therapists journal,* vol. 39, no. 3, pp. 15-19, 2019.

[9] T. Virgin-Elliston, P. Nonboe, E. B. Boisen, and H. Koblauch, "Evaluating the Performance and Perception of a Stoma Bag Full-Circle Filter in People with a Colostomy or an Ileostomy—Two Randomized Crossover Trials," *Healthcare,* vol. 11, no. 3, p. 369, 2023.

[10] H. Brown and J. Randle, "Living with a stoma: a review of the literature," (in eng), *J Clin Nurs,* vol. 14, no. 1, pp. 74-81, Jan 2005.

[11] S. Ayaz-Alkaya, "Overview of psychosocial problems in individuals with stoma: A review of literature," (in eng), *International wound journal,* vol. 16, no. 1, pp. 243-249, 2019.

[12] A. Bloemen, F. Aarts, N. Bouvy, and P. Nijhuis, "Evaluation of a New Elastic Ostomy Appliance to Decrease Skin Complications: Results of a Pilot Study," (in eng), *Wound Manag Prev,* vol. 66, no. 5, pp. 30-36, May 2020.

[13] S. K. O'Flynn, "Peristomal skin damage: assessment, prevention and treatment," (in eng), *Br J Nurs,* vol. 28, no. 5, pp. S6-s12, Mar 14 2019.

[14] T. Winslow, "[Sequential illustration of colon cancer diagnosis, colostomy procedure, and colostomy bag placement]," ed. Galliano Surgical Group, 2005.

[15] D. Wechter. "Changing your ostomy pouch." https://medlineplus.gov/ency/patientinstructions/000204.htm (accessed 2023).
[16] D. Anisuzzaman, C. Wang, B. Rostami, S. Gopalakrishnan, J. Niezgoda, and Z. Yu, "Image-based artificial intelligence in wound assessment: A systematic review," *Advances in Wound Care,* vol. 11, no. 12, pp. 687-709, 2022.
[17] Y. Lucas, R. Niri, S. Treuillet, H. Douzi, and B. Castaneda, "Wound size imaging: ready for smart assessment and monitoring," *Advances in wound care,* vol. 10, no. 11, pp. 641-661, 2021.
[18] R. Styliński, A. Alzubedi, and S. Rudzki, "Parastomal hernia–current knowledge and treatment," *Videosurgery and Other Miniinvasive Techniques,* vol. 13, no. 1, pp. 1-8, 2018.
[19] E. Polsinelli. "ConvaTec SUR-FIT Natura Moldable: REVIEW (w/ video)." [Online]. Available: https://www.veganostomy.ca/convatec-moldable-review/#What_exactly_is_a_moldable_wafer (accessed 2023).
[20] E. Polsinelli. "Hollister FormaFlex Moldable Wafer: REVIEW (w/ video)." [Online]. Available: https://www.veganostomy.ca/hollister-formaflex/ (accessed 2023).
[21] Ravikanth. "Advancements in Ostomy Systems." [Online]. [Online]. Available: https://www.patent-art.com/knowledge-center/advancements-in-ostomy-systems/ (accessed 2023).
[22] OstomyCure. "OstomyCure." [Online]. Available: https://ostomycure.com/ (accessed 2023).
[23] S. Wang *et al.*, "A new smart mobile system for chronic wound care management," *IEEE Access,* vol. 6, pp. 52355-52365, 2018.
[24] T. W. K. Poon and M. R. Friesen, "Algorithms for Size and Color Detection of Smartphone Images of Chronic Wounds for Healthcare Applications," *IEEE Access,* vol. 3, pp. 1799-1808, 2015.
[25] U. Pavlovčič and M. Jezeršek, "Handheld 3-dimensional wound measuring system," *Skin Research & Technology,* Article vol. 24, no. 2, pp. 326-333, 2018.
[26] V. Mamone, M. D. Fonzo, N. Esposito, M. Ferrari, and V. Ferrari, "Monitoring Wound Healing With Contactless Measurements and Augmented Reality," *IEEE Journal of Translational Engineering in Health and Medicine,* vol. 8, pp. 1-12, 2020.
[27] D. Sánchez-Jiménez, F. F. Buchón-Moragues, B. Escutia-Muñoz, and R. Botella-Estrada, "SfM-3DULC: Reliability of a new 3D wound measurement procedure and its accuracy in projected area," *International wound journal,* vol. 19, no. 1, pp. 44-51, 2022.
[28] E. Sirazitdinova and T. M. Deserno, "System design for 3D wound imaging using low-cost mobile devices," in *Medical Imaging 2017: Imaging Informatics for Healthcare, Research, and Applications*, 2017, vol. 10138: SPIE, pp. 258-264.
[29] A. F. M. Hani, N. M. Eltegani, S. H. Hussein, A. Jamil, and P. Gill, "Assessment of Ulcer Wounds Size Using 3D Skin Surface Imaging." Berlin, Heidelberg: Berlin, Heidelberg: Springer Berlin Heidelberg, pp. 243-253.
[30] M. Mizoguchi, M. Kayaki, T. Yoshikawa, M. Asano, K. Onishi, and H. Noborio, "Selection and Evaluation of Color/Depth Camera for Imaging Surgical Stoma," in *Human-Computer Interaction. Interaction Techniques and Novel Applications*, Cham, M. Kurosu, Ed., 2021// 2021: Springer International Publishing, pp. 601-614.
[31] D. Filko, R. Cupec, and E. K. Nyarko, "Wound measurement by RGB-D camera," *Machine Vision and Applications,* vol. 29, no. 4, pp. 633-654, 2018/05/01 2018.

[32] A. Shah, C. B. Wollak, and J. B. M. C. Shah, "Wound Measurement Techniques: Comparing the Use of Ruler Method, 2D Imaging and 3D Scanner," *The journal of the American College of Clinical Wound Specialists,* vol. 5, no. 3, pp. 52-57, 2015.
[33] A. Yee, F. Meng, S. Yi, and J. Harmon, "An Innovative App for the Management of Chronic Wound Treatment," in *2018 IEEE/ACM International Conference on Connected Health: Applications, Systems and Engineering Technologies (CHASE)*, 26-28 Sept. 2018 2018, pp. 3-4.
[34] L. B. Jørgensen, J. A. Sørensen, G. B. Jemec, and K. B. Yderstraede, "Methods to assess area and volume of wounds - a systematic review," (in eng), *International wound journal,* vol. 13, no. 4, pp. 540-553, 2016.
[35] J. M. Juszczyk *et al.*, "Wound 3D Geometrical Feature Estimation Using Poisson Reconstruction," *IEEE Access,* vol. 9, pp. 7894-7907, 2021.
[36] D. F. Redaelli, S. G. Barsanti, E. Biffi, F. A. Storm, and G. Colombo, "Comparison of geometrical accuracy of active devices for 3D orthopaedic reconstructions," *The International Journal of Advanced Manufacturing Technology,* vol. 114, no. 1, pp. 319-342, 2021/05/01 2021.
[37] S. Zahia, B. Garcia-Zapirain, J. Anakabe, J. Ander, O. Jossa Bastidas, and A. Loizate Totoricagüena, "A Comparative Study between Scanning Devices for 3D Printing of Personalized Ostomy Patches," *Sensors,* vol. 22, no. 2, 2022.
[38] G. Guidi, S. Gonizzi, and L. Micoli, "3D CAPTURING PERFORMANCES OF LOW-COST RANGE SENSORS FOR MASS-MARKET APPLICATIONS," *Int. Arch. Photogramm. Remote Sens. Spatial Inf. Sci.,* vol. XLI-B5, pp. 33-40, 2016.
[39] T. P. Kersten, M. Lindstaedt, and D. Starosta, "COMPARATIVE GEOMETRICAL ACCURACY INVESTIGATIONS OF HAND-HELD 3D SCANNING SYSTEMS – AN UPDATE," *Int. Arch. Photogramm. Remote Sens. Spatial Inf. Sci.,* vol. XLII-2, pp. 487-494, 2018.
[40] M. Farhan, J. Z. Wang, J. Lillia, T. L. Cheng, and J. Burns, "Comparison of multiple 3D scanners to capture foot, ankle, and lower leg morphology," *Prosthetics and Orthotics International*.
[41] G. Guidi, M. Russo, G. Magrassi, and M. Bordegoni, "Performance Evaluation of Triangulation Based Range Sensors," *Sensors,* vol. 10, no. 8, pp. 7192-7215, 2010.
[42] All3DP. "The Best Cheap 3D Scanners in 2023." [Online]. Available: https://all3dp.com/1/best-cheap-3d-scanners-low-budget/ (accessed 2023).
[43] M. Griggs. "The best 3D scanners in July 2023." [Online]. Available: https://www.creativebloq.com/buying-guides/best-3d-scanners (accessed 2023).
[44] All3DP. "The Best 3D Scanners in 2023 – Buyer's Guide." [Online]. Available: https://all3dp.com/1/best-3d-scanner-diy-handheld-app-software/ (accessed 2023).
[45] "Primesense Carmine 1.09." [Online]. Available: http://xtionprolive.com/primesense-carmine-1.09 (accessed 2023).
[46] "Xtion Pro Live." [Online]. Available: http://xtionprolive.com/asus-xtion-pro-live (accessed 2023).
[47] "Creaform HandySCAN 3D 700." [Online]. Available: https://3dscannertech.com/creaform-3d-laser-scanners/creaform-handyscan-3d-700 (accessed 2023).

[48] "Creality CR-Scan 01 3D Scanner Set-400-900mm Scanning Range, No Maker Scanning." [Online]. Available: https://www.creality3dofficial.com/products/creality-cr-scan-01-3d-scanner-set (accessed 2023).
[49] "CR-Scan Ferret." [Online]. Available: https://www.creality.com/products/cr-scan-ferret-3d-scanner (accessed 2023).
[50] "Shining 3D FreeScan X7 3D Scanner." [Online]. Available: https://top3dshop.com/product/shining-3d-freescan-x7-3d-scanner (accessed 2023).
[51] "GOM ATOS II Triple Scan, TRITOP 4 System 3D Scanner." [Online]. Available: https://www.primeanalyzerstore.com/product/gom-atos-ii-triple-scan-tritop-4-system-3d-scanner/ (accessed 2023).
[52] I. RealSense. "Intel® RealSense™ Depth Camera D435." [Online]. Available: https://www.intelrealsense.com/depth-camera-d435/ (accessed 2023).
[53] P. Miller. "The iPhone X's notch is basically a Kinect." [Online]. Available: https://www.theverge.com/circuitbreaker/2017/9/17/16315510/iphone-x-notch-kinect-apple-primesense-microsoft (accessed 2023).
[54] "Buy iPhone 12." [Online]. Available: https://www.apple.com/shop/buy-iphone/iphone-12/6.1-inch-display-64gb-black-unlocked (accessed 2023).
[55] K. Minolta. "NON-CONTACT 3D DIGITIZER VIVID 9i/VI-9i.". [Online]. Available: https://www.konicaminolta.com/instruments/download/instruction_manual/3d/pdf/vivid-9i_vi-9i_instruction_eng.pdf (accessed 2023).
[56] K. Balderson. "10 Best 3D Scanners for 2023." [Online]. Available: https://techjury.net/best/3d-scanners/ (accessed 2023).
[57] Rodin4D. "3D Scanners." rodin4d.com. [Online]. Available: https://www.rodin4d.com/en/scanner-3d-professionnel/ (accessed 2023).
[58] top3dshop. "3D Systems Sense 2 3D scanner." [Online]. Available: https://top3dshop.com/product/3d-systems-sense-2-3d-scanner (accessed 2023).
[59] Tim. "Shining 3D Einstar Review: Handheld Scanning on a Budget." https://clevercreations.org/shining-3d-einstar-3d-scanner-review/ (accessed 2023).
[60] "Structure Sensor Pro." https://structure.io/structure-sensor-pro (accessed 2023).
[61] C.-Y. Chiu, M. Thelwell, T. Senior, S. Choppin, J. Hart, and J. Wheat, "Comparison of depth cameras for three-dimensional reconstruction in medicine," *Proceedings of the Institution of Mechanical Engineers, Part H: Journal of Engineering in Medicine,* vol. 233, no. 9, pp. 938-947, 2019.
[62] F. Laricchia. "Share of smartphone users that use an Apple iPhone in the United States from 2014 to 2022." statista.com. [Online]. Available: https://www.statista.com/statistics/236550/percentage-of-us-population-that-own-a-iphone-smartphone/ (accessed 2023).
[63] A. Essop. "Samsung unveils new Galaxy Note 10 model with "instant" 3D scanning capabilities." [Online]. Available: https://3dprintingindustry.com/news/samsung-unveils-new-galaxy-note-10-model-with-instant-3d-scanning-capabilities-159877/ (accessed 2023).
[64] M. deAgonia. "Apple's Face ID [The iPhone X's facial recognition tech] explained | Computerworld." [Online]. Available: https://www.computerworld.com/article/3235140/apples-face-id-the-iphone-xs-facial-recognition-tech-explained.html (accessed 2023).

[65] Apple. "About Face ID advanced technology." [Online]. Available: https://support.apple.com/en-us/HT208108 (accessed 2023).
[66] *InfiniTAM_ios*. (2022). GitHub repository. [Online]. [Online]. Available: https://github.com/neycyanshi/InfiniTAM_ios
[67] eyeryscompany, "How Apple's LiDAR Sensor Differs From The One On Its 'TrueDepth' Face ID | Eyerys," 2020-03-30 2020.
[68] J. Stillman. "The Fascinating Reason Why Blue Is the World's (and Brands') Favorite Color." https://www.inc.com/jessica-stillman/the-fascinating-science-of-why-so-many-brands-have-blue-logos.html (accessed 2023).
[69] O. Kähler, V. A. Prisacariu, C. Y. Ren, X. Sun, P. Torr, and D. Murray, "Very high frame rate volumetric integration of depth images on mobile devices," *IEEE transactions on visualization and computer graphics,* vol. 21, no. 11, pp. 1241-1250, 2015.
[70] "Firebase Documentation." https://firebase.google.com/docs (accessed 2023).
[71] S. Suzuki, "Topological structural analysis of digitized binary images by border following," *Computer vision, graphics, and image processing,* vol. 30, no. 1, pp. 32-46, 1985.
[72] Vata. "REPLACEMENT STOMA PACKAGE - VATA." [Online]. Available: https://vatainc.com/product/replacement-advanced-stoma-package/ (accessed 2023).
[73] "OpenCV: Structural Analysis and Shape Descriptors." [Online]. Available: https://docs.opencv.org/3.4/d3/dc0/group__imgproc__shape.html#ga17ed9f5d79ae97bd4c7cf18403e1689a (accessed 2023).
[74] N. Otsu, "A threshold selection method from gray-level histograms," *IEEE transactions on systems, man, and cybernetics,* vol. 9, no. 1, pp. 62-66, 1979.
[75] "OpenCV: Smoothing Images." [Online]. Available: https://docs.opencv.org/4.x/d4/d13/tutorial_py_filtering.html (accessed 2023).
[76] E. Arias-Castro and D. L. Donoho, "Does median filtering truly preserve edges better than linear filtering?," 2009.
[77] G. B. Turnbull. "Ostomy Statistics: The $64,000 Question." HMP Communications. [Online]. Available: http://www.o-wm.com/content/ostomy-statistics-the-64000-question (accessed 2023).
[78] Byram Healthcare, "Ostomy Catalog | 2023". [Online]. Available: https://www.byramhealthcare.com/-/media/catalog/byram-healthcare-ostomy-supplies-catalog.pdf.